UNIVERSITAT POLITÈCNICA DE CATALUNYA
BARCELONATECH
Escola Superior d'Enginyeries Industrial,
Aeroespacial i Audiovisual de Terrassa

TREBALL DE FI D'ESTUDIS

Large Eddy Simulations of wind turbines using the Actuator Disc model implemented in Alya

Document:

Report

Author:

Eva Peinado Montoya

Director - Codirector:

Prof. Ivette Maria Rodriguez Perez

Dr. Matías Oscar Ávila Salinas

Dr. Angel Herbert Owen Coppola

Degree:

Master's degree in Aerospace Engineering

Call:

Spring semester, 2022

Abstract

The main objective of this project is to validate the wake generated behind a wind turbine with Large Eddy Simulation (LES). LES is currently the preferred technique for performing high-fidelity numerical simulations of flows around wind turbines, and is the one used in this work in order to characterise the wake generated by the wind turbine. The cases under study are a surface boundary layer and a single wind turbine case. Several methods are available to simulate the rotor, and actuator disc is the one implemented due to its low computational cost, making it the preferred option for wind turbine wake studies. The actuator disc models the effect of the wind turbine as an external force acting over the area covered by the rotor. A study on three different actuator disc forces is also done: a constant force, a force depending on the undisturbed wind velocity, and a force depending on the integrated velocity directly at the disc. The force chosen to validate the results is the force calculated with the undisturbed wind velocity, since it is proven to provide more real results. Validation is done by comparing the results of the wind turbine wake with those from the reference. Results show good agreement with the reference for low turbulence intensities, but are not reliable for higher turbulence intensities due to the difficulty of arriving to the statistical steady state. The simulations are performed with Alya, the multiphysics simulation HPC code developed at the Barcelona Supercomputing Center. It has been used for wind energy simulations for more than ten years, making it a robust option for wind applications.

Resumen

El objetivo principal de este proyecto es validar la estela generada por una turbina eólica con Large Eddy Simulation (LES). LES es actualmente la técnica preferida para llevar a cabo simulaciones numéricas de alta fidelidad de flujos alrededor de turbinas eólicas, y es el que se ha utilizado en este proyecto para caracterizar la estela generada. Los casos estudiados son una capa límite superficial y una única turbina eólica. Existen varios métodos para modelar el rotor de la turbina, y el disco actuador es el implementado debido a su bajo coste computacional, haciendo que sea la opción preferida para estudios de turbinas eólicas. El modelo de disco actuador modela el efecto de la turbina eólica como una fuerza externa actuando sobre el área cubierta por el rotor. También se lleva a cabo un estudio de tres fuerzas distintas de disco actuador: una fuerza constante, una fuerza calculada con la velocidad no perturbada y una fuerza calculada con la velocidad integrada directamente en el disco. De estas tres, la fuerza elegida para validar los resultados es la fuerza calculada con la velocidad no perturbada, ya que ofrece valores más similares a la realidad. La validación se realiza comparando los resultados obtenidos de la estela de la turbina eólica con los disponibles de referencia. Los resultados muestran concordancia con la referencia para casos de baja intensidad turbulenta, pero dejan de ser fiables para casos de alta intensidad turbulenta debido a la dificultad de llegar al estado estacionario estadístico. Las simulaciones se han llevado a cabo con Alya, el código multifísico de simulación de alta eficiencia computacional desarrollado en Barcelona Supercomputing Center. Este código se ha utilizado para simulaciones de energía eólica más de 10 años, haciendo que sea una opción fiable para aplicaciones de viento.

Acknowledgements

I would like to thank my co-tutor Matías, who has helped me throughout all the process of the project and it would not have been possible without him. Without a doubt, he has been the main support in these four months and I will be grateful forever. Other important roles in this project are my co-tutor Herbert and my tutor Ivette, who helped me to substantially improve the work done with their advice.

I would also like to thank my family and Ana, that were my emotional and unconditional support in these months.

Finally, I would like to thank the Universitat Politècnica de Catalunya and Barcelona Supercomupting Center for giving me the opportunity of doing this project, which was a very enriching experience.

Contents

List of Figures

List of Tables

List of abreviations

LES Large Eddy Simulation I

CFD Computational Fluid Dynamics 1

ABL Atmospheric Boundary Layer 3

RANS Reynolds-averaged Navier-Stokes 3

Chapter 1

Introduction

Renewable energies are starting to play a major role in terms of energy production. The combination of climate change and the lack of fossil fuels is imposing a transition towards clean energies, where wind energy plays a major role. In Europe, wind industry increased its power capacity a 18% in 2021 with respect to 2020, a rate that is expected to grow in order to achieve the 2030 Climate and Energy goals. More specifically, in Spain 24% of the total electrical energy consumed in 2021 came from wind farms [1]. Therefore, it is a topic of high interest to study the efficiency of wind parks and subject to continuous improvement.

Wind farms are formed by wind turbines, which are usually placed close to each other due to the reduced availability of ideal locations and the maximisation of economic profitability of the land. The vicinity of wind turbines causes interference, not only with the turbines themselves but also with the air surrounding them, and thus creating a wake. Wind turbine wakes increase the level of turbulence, which translates into energy losses estimated on 20% on flat terrain and possible effects on the structural integrity of the turbines. Therefore, a better understanding of the turbulent flow is needed to reduce these losses, make wind energy cheaper and make it widespread accessible.

For the characterisation of turbulence, Computational Fluid Dynamics (CFD) is a powerful tool which makes possible to solve the behaviour of fluids. In particular, CFD is used in the present work to solve the behaviour of atmospheric air around wind turbines using LES, a turbulence model of Navier-Stokes equations.

1.1 Objective

The main objective of this project is to validate and characterise the flow around wind turbines using LES with actuator disc model and Alya software. In order to achieve the main objective, some more specific objectives have been defined:

- Familiarisation with Alya high-performance code, learning how to use it and the range of different options.
- Knowledge on the meshing procedure in order to obtain reliable results.
- Surface boundary layer flow characterisation.

- Single-wake flow characterisation.
- Comprehension of the wind flow and turbulence structures upwind, downwind, and surrounding the wind turbine.

1.2 Scope

To deliver the work proposed, it will be necessary to complete the following three main work packages:

1. Simulation of a surface boundary layer, with its characterisation.
2. Simulation of a single wind turbine, with its characterisation.
3. Validation of the results of a single wind turbine.

1.3 Requirements

The requirement to complete this work is basically the availability of a computer with high-computational capacity like MareNostrum IV or Nord3 supercomputers, in which is possible to simulate domains with elevated number of elements and high Reynolds numbers.

1.4 Justification

This project arises from the need of an energetic transition, from energy extracted from fossil fuels to a clean and renewable energy, in which wind energy plays a major role. The unstoppable increasing temperatures around the globe in combination with the lack of fossil fuels, are making a priority to design a new energy model which is formed by energies that, in the process of converting energy, do not emit, or emit minimum amounts, of any greenhouse or pollutant gases to the atmosphere.

Wind energy is becoming one of the most important renewable energies due to its simplicity and reliability. However, the interference between wind turbines affects the total efficiency of wind farms, reason why its behaviour is being constantly investigated. The complete knowledge of the wind behaviour going through the wind turbines will make possible to evaluate and optimise the production of wind farms.

Simulations of large Reynolds number flows with LES have been limited until now. However, due to the higher capacity of supercomputers, it is possible now to carry out LES of larger computational domains at high Reynolds numbers.

Chapter 2

State of the art

Simulations of wind farms with CFD models imply to solve the Atmospheric Boundary Layer (ABL) in a turbulent regime, as well as the effects produced by wind turbines. These effects include wind speed deficit, increase of turbulent kinetic energy, and interaction among wakes [2]. However, the characterisation of these effects can be done through different techniques that have been in evolution in terms of computational capacity. Along this chapter, a brief state of the art of the CFD models will be done to introduce the most used techniques to perform these type of CFD simulations, in order to place the project in the current framework.

When talking about wind turbine CFD simulations, three main fields will define the problem: the turbulence model, the rotor model and the numerical method to discretise the Navier-Stokes equation. In the following sections, the current tendency of each of these topics is going to be explained.

2.1 Turbulence model

When working with CFD simulations, Navier-Stokes equations are closed with a turbulence model. The two most important methodologies in turbulence modelling for wind flow in the presence of wind turbines are RANS and LES [3].

On one hand, Reynolds-averaged Navier-Stokes (RANS) methods have been widely used in the past years. These equations look for a statistical description of the flow, describing flow characteristics such as pressure and velocity as time average values and a variance [3]. For solving them, an extra equation for the RANS model must be implemented to finally calculate the turbulent 'eddy' viscosity. One of the most used methods to obtain this variable is the $k-\epsilon$ RANS model. However, this model is overdiffusive, which causes underestimations in the wake length. However, the new model $k-\epsilon-f_p$ introduces a correction to the previous method, obtaining lower mixing lengths in the wake region. This makes it more precise and is able to describe the near wake turbulence [4].

On the other hand, LES is gaining popularity due to its ability of describing unsteady, anisotropic turbulent flows dominated by large-scale structures and turbulent mixing [3]. This turbulence model solves the velocity field up to a certain eddy scale, and models the smaller scales. In comparison to RANS, the implementation of this model needs higher computational

costs because of the use of finer meshes and time step sizes in order to obtain reliable results. However, due to the increasing computational capacity in the past years, the use of LES models with finer meshes is more accessible.

Comparing both turbulence models, $k-\varepsilon$ without corrections tends to under-predict the wake deficit at all downstream distances from the turbine and overestimate the turbulence intensity. On the other hand, the $k-\varepsilon-f_p$ RANS model is able to describe the wake deficits in the near region more precisely, but does not provide good results for the far wake. However, LES has been proven to provide reliable results, comparing them with the ones obtained experimentally [4].

LES is able to provide more accurate solutions of the flow if the resolved turbulence scales are small enough to properly represent the effects of eddies and flow fluctuations. However, due to computational limitations LES has not been widely used until recent years, but with the computational capacity of computer clusters nowadays it is becoming a very useful and affordable tool to solve the wind flow in the presence of wind turbines, also above very complex terrain [5]. In the work of Van der Laan et al. [4], LES results are used to compare them with RANS results and with measurements, and it gives very accurate results.

2.2 Rotor modelling

Regarding the rotor description in CFD simulations, four main types can be found to represent wind turbines: full rotor, engineering wake models, actuator line and actuator disc.

The full rotor model is the one that demands higher computational cost. It consists on fully representing the geometry of the wind turbine, creating an adapted curvilinear mesh. This model needs to solve the flow surrounding the wind turbine blade, being useful when studying the design of turbine blades, but too expensive for wind farm modelling.

The engineering wake models, on the other hand, are the cheapest rotor model since they impose an analytical velocity wake deficit and therefore do not resolve the wake, but model it with momentum conservation. When having several wind turbines, the interaction between them is also modelled through linear superposition. This method provides a good balance between the accuracy of results and capturing the turbine power, and the computational cost, and give very reliable results for offshore applications. However, the main drawbacks are the need of knowing the velocity wake deficit, which should be previous to the implementation of the model, and the difficulty of applying it in complex terrain.

The actuator line model is an intermediate point regarding computational cost. It is based on modelling the turbine blades as lines, which apply a force to the wind applying the lift and drag coefficients of the blade profile, representing in a certain way the blade geometry.

Finally, the actuator disc model is the computationally simpler one, since it models the turbine as a disc applying a force to the wind. The force implemented is distributed in the disc and has an axial component, including sometimes a tangential component too, for rotation simulation. The blade geometry can also be implemented through the corresponding lift and drag coefficients in order to obtain the force, distributed over the disc. However, it is also possible to not know the blade geometry and impose directly the thrust coefficient given

by the manufacturer. Although it is a very simple model, it provides results similar to the ones obtained by the actuator line model for the mid and far wake. More specifically, the implementation of actuator discs can help to reduce the computational cost when running LES simulations.

2.3 Numerical method

Different numerical methods can be found nowadays to solve Navier-Stokes equations. One of the most popular codes is OpenFoam, which uses a finite volume numerical method to solve the equations. Ellypsis3D is another solver that employs finite volume method, created by DTU. In this work, Alya is the used code, which is the in-house High Performance Computing code developed in Barcelona Supercomputing Center. Alya uses a stabilised finite element model, with same shape functions for velocity and pressure. It has implemented several turbulence models for the Navier-Stokes equations, such as RANS, URANS and LES [2].

Chapter 3

Methodology

3.1 Governing equations

The Navier Stokes equations describe the wind flow dynamics inside the ABL, since it is a viscous fluid. These equations ensure the conservation of momentum and conservation of mass, shown in Equation 3.1 and Equation 3.2 respectively, considering an incompressible fluid with constant density and dynamic viscosity μ.

$$\rho\frac{\partial \mathbf{u}}{\partial t} + \rho\mathbf{u}\cdot\nabla\mathbf{u} = -\nabla\mathbf{p} + \nabla\cdot(2\mu\varepsilon(\mathbf{u})) + \mathbf{f} \tag{3.1}$$

$$\nabla\cdot\mathbf{u} = 0 \tag{3.2}$$

where $\mathbf{u}$ and $\mathbf{p}$ are the velocity and pressure fields respectively, which are the unknowns of the equation. Then t is the time, ρ is the density of the fluid, μ is the dynamic viscosity, $\varepsilon(u)$ is the symmetric gradient operator, which gives the velocity strain rate tensor and is defined as $\varepsilon(u) = \frac{1}{2}\left(\nabla\mathbf{u} + \nabla^T\mathbf{u}\right)$, and $\mathbf{f}$ is a force field per unit volume.

The solution of Navier-Stokes equations can be analytically obtained for very simple cases, but when the problem is more complicated, a numerical method must be applied in order to obtain a solution. This numerical method should achieve the maximum accuracy when solving the momentum and mass conservation equations, which translates into a fine enough discretization in order to capture all the scales of the flow. However, computational costs increase with the Reynolds number, so it is necessary to apply a model in which empirical modelling is used to approximate turbulent effects. In particular, the method applied in this work is Large Eddy Simulations (LES).

3.1.1 LES equations

Large Eddy Simulations (LES) differentiates between the large, energy-containing scales and the smallest ones by means of a low-pass filtering operation. The largest scales that are above the filtering threshold are resolved, and their interaction with the smallest scales is modelled. This scale separation is done by decomposing the velocity field according to Equation 3.3.

$$\mathbf{u}_i = \overline{\mathbf{u}_i} + \mathbf{u}_{SGS} \tag{3.3}$$

where $\bar{\mathbf{u}}_i$ is the filtered component, and $\mathbf{u}_{SGS}$ is the subgrid component.

The filtering process is achieved through a spatial filtering process, which is obtained by the convolution of the instantaneous field and the certain type of filter. In wind energy applications, the most common used filter is the implicit filtering since its width is associated to the grid size. Applying the filtering procedure to Navier-Stokes Equations 3.1 and 3.2, it is possible to obtain Equations 3.4 and 3.5.

$$\rho\frac{\partial\bar{\mathbf{u}}}{\partial t} + \rho\bar{\mathbf{u}}\cdot\nabla\bar{\mathbf{u}} = -\nabla\bar{p} + \nabla\cdot(2\mu\varepsilon(\bar{\mathbf{u}})) + \bar{\mathbf{f}} - \nabla\cdot\tau^{SGS} \tag{3.4}$$

$$\nabla\bar{\mathbf{u}} = 0 \tag{3.5}$$

where $\tau^{SGS} = -\rho(\overline{u_i u_j} - \bar{u}_i\bar{u}_j)$ is the stress tensor coming from the non-linearity of the convection term and expresses the effect of the modelled scales on the solved ones. This turbulent stress tensor is modelled assuming the following subgrid turbulent viscosity model.

$$\tau_{ij}^{SGS} = -2\mu_{SGS}\overline{\varepsilon_{ij}} \tag{3.6}$$

In the present work the Vreman subgrid viscosity model is applied [6].

3.2 Actuator disc model

The actuator disc model is an idealised rotor representation in which it is assumed to have an infinite number of blades, the force per unit area is radially distributed and azimuthally homogeneous, and there is no wake rotation [7]. For this particular case, the force per unit area is axial and uniformly distributed over the disc. In Figure 3.1 the actuator disc model is represented, showing the change in the velocity which causes a pressure jump along the disc thickness inside the control volume of the disc. The force per unit volume generated by the disc is defined in Equation 3.7.

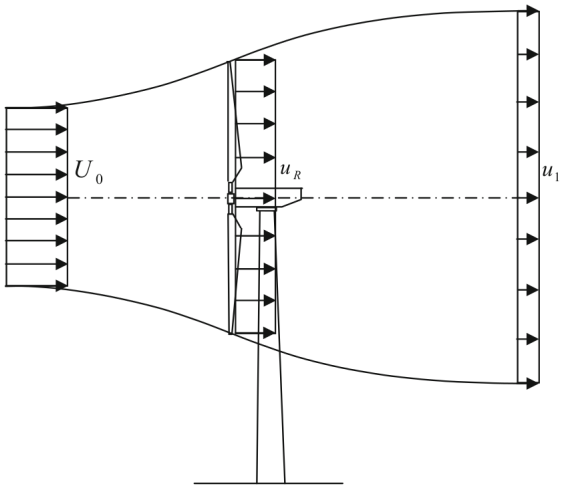

Figure 3.1: Control volume for one-dimensional actuator disc [7]

$$\mathbf{f} = \frac{1}{2}\rho\frac{C_t}{\Delta}U_{H,\infty}^2\hat{\mathbf{n}} \tag{3.7}$$

where C_t is the thrust coefficient, $U_{H,\infty}$ is the undisturbed wind velocity, Δ is the thickness of the disc and $\hat{n}$ is the unit normal vector of the disc, in opposite direction to the wind flow.

Regarding the thrust coefficient, it is usually given by the manufacturers in terms of the undisturbed wind velocity $U_{H,\infty}$.

3.2.1 Calculation of undisturbed wind velocity $U_{H,\infty}$

The actuator disc force depends directly on the undisturbed wind velocity at hub height $U_{H,\infty}$, and manufacturers usually provide the thrust coefficient C_t in terms of this variable $U_{H,\infty}$. However, the free stream velocity is not always easy to obtain. Three different methods to calculate the actuator disc force have been studied in this work.

The first method consists on assuming a constant undisturbed wind velocity $U_{H,\infty}$ which, consequently, imposes a constant force. This force does not change with time so it does not adapt to the changes of velocity. Consequently, when the undisturbed wind velocity changes with small frequencies, the wake size will change, since the force will be the same. For example, if the velocity upstream the disc decreases, the force will be respectively higher, thus creating a higher wake.

The second method consists of using the undisturbed wind velocity as the wind velocity at hub height at a distance of 3 diameters upstream from the disc. This velocity is considered to be out of the induction zone and therefore, can be considered as undisturbed, meaning that $U_{H,\infty} = U_{H,3D}$. The force is then directly computed in terms of this velocity, which is a realistic approximation over flat terrains.

The third method to obtain the undisturbed wind velocity $U_{H,\infty}$ is by making the integral of the horizontal velocity at the disc and calculating the average. Then, it is divided by its volume and averaged in one minute. This velocity is considered as U_{hub} and it is related

with the undisturbed wind velocity through the induction factor a, indicated in Equation 3.8. Applying one-dimensional momentum theory, the expression for the thrust coefficient $C_t = 4a(1-a)$ can be found. However, this relation is only valid up to $a < 0.4$. When this value is exceeded, C_t is obtained through Glauert empirical law, as in Equation 3.9 [7].

$$a = 1 - \frac{U_{hub}}{U_{H,\infty}} \tag{3.8}$$

$$C_{ta}(a) = \begin{cases} 4a(1-a) & a < 0.4 \\ 0.889 - (0.0203 - (a-0.143)^2)/0.6427 & a \geq 0.4 \end{cases} \tag{3.9}$$

When using Equations 3.9 and 3.8, an iterative process usually is started based on an initial guess of $U_{H,\infty}$. In the first place, a C_{tm} is determined in terms of $U_{H,\infty}$ from the manufacturer given data. Then, a is obtained from Equation 3.9 and $U_{H,\infty}$ can be updated from equation 3.8. This procedure is repeated until $U_{H,\infty}$ converges to a fixed value (and verifying that $C_{ta} = C_{tm}$), translated into Equation 3.10, in which the one-dimensionality of the problem is exploited and it can be solved using the bisection method [2].

$$f(U_{H,\infty}) = C_{tm}(U_{H,\infty}) - C_{ta}\left(1 - \frac{U_{hub}}{U_{H,\infty}}\right) \tag{3.10}$$

3.3 Cases of study

The cases that are going to be under study in the present work are two: the first case is surface boundary layer flow, and the second one is a wind turbine immersed in surface boundary layer.

3.3.1 Surface Boundary Layer case

The first case of study is a surface boundary layer flow, the lowest part of the ABL in which the velocity profile depends on the distance from the wall. In this case, the problem domain is a three-dimensional box $\Omega = [-0.4L_x, 0.6L_x] \times [-0.5L_y, 0.5L_y] \times [0, L_z]$, where $L_x = 10000m$, $L_y = 5000m$ and $L_z = 1000m$ are the lengths in the streamline, streamwise and vertical direction respectively. The domain dimensions have been obtained through an iterative process in which the main concern was that its size is large enough such that all the structures of the flow are completely developed.

Boundary conditions

The domain is a box with six faces containing the volume under study. In this section, the boundary conditions that define the characteristics of the flow are going to be defined.

- The lateral boundaries, at $x = -0.4L_x$, $x = 0.6L_x$, $y = -0.5L_y$ and $y = 0.5L_y$ are periodic.

- The top boundary, at $z = L_z$, has symmetry boundary condition. That is, it satisfies the non penetration condition $\mathbf{u} \cdot \mathbf{n} = 0$, and zero shear stress at the top.
- Finally, at the bottom boundary, $z = 0$, we use a wall model that relates the wall shear stress τ_w with the horizontal velocity at a distance δ_w from the wall. The wall model that we use is the classic Monin-Obukhov similarity theory for neutral boundary layers [2]. This wall stress boundary condition is only dependent on the surface roughness z_0

$$|\mathbf{u}_t(\delta_w)| = \frac{u_*}{\kappa} ln\left(\frac{\delta_w + z_0}{z_0}\right) \tag{3.11}$$

$$\tau_w = -\rho u_*^2 \frac{\mathbf{u}_t}{|\mathbf{u}_t|} \tag{3.12}$$

where κ is the Von Kármán constant that we adopt as $\kappa = 0.41$, z_0 is the wall roughness, u_* is the friction velocity, $\mathbf{u}_t$ is the velocity component tangential to the wall, and ρ is the air density.

Initial conditions

The initialisation of the numerical simulation is done by imposing at the initial time a logarithmic profile with known velocity U at a certain height. To this velocity profile, random fluctuation are added to simulate perturbations. Then, the velocity profile imposed can be divided as follows.

$$u = \bar{u} + u_{random} \tag{3.13}$$

These random perturbation term takes amplitudes 5% from those of the wind speed $\bar{u}$. They are applied at the initialisation of the problem, and then the flow is developed until achieving to a statistical steady state.

Setting of the case

We will set the case such we obtain a wind profile with a certain wind speed U_H. and turbulence intensity TI at a given height.

The turbulence intensity TI is defined as the ratio between the root-mean-square of the velocity fluctuations u',v',w' and the wind speed, as follows

$$TI = \frac{\sqrt{\frac{1}{3}(u'u' + v'v' + w'w')}}{U} \tag{3.14}$$

where $\overline{u}$, v and w are the velocities components, and u', v' and w' are the velocity fluctuations, in x, y and z directions respectively. U is the mean wind speed. However, this TI is difficult to set, due to its dependence on the velocity field, which is the unknown of the problem. We assume that the TI profile follows Equation 3.15, which is the TI profile obtained using a $k - \varepsilon$ RANS model.

$$TI(z) = \frac{\kappa\sqrt{\frac{2}{3}}}{\ln\left(\frac{z+z_0}{z_0}\right)\sqrt[4]{C_\mu}} \tag{3.15}$$

where C_μ is a constant with value $C_\mu = 0.03$. The defined value for this surface boundary layer test case of the turbulence intensity is $TI = 12.8\%$.

The other parameter defining the case is an imposed velocity at a certain height which in this case is of $U_{H,\infty} = 8m/s$ at $z = 90m$. The imposition of this TI and this velocity define the first estimation of the bottom wall roughness, which can be extracted from Equation 3.15. In this case, the imposed roughness of the bottom wall is $z_0 = 0.1682m$.

In order to have the flow at related imposed momentum conservation over the entire domain, a balance of forces is done. In the domain, two forces are acting on the flow: the first one is the shear force generated at the bottom wall F_τ and defined in Equation 3.16, and the second one is a driven pressure force F_p, defined in Equation 3.17.

$$F_p = \nabla p \cdot L_z \cdot L_y \tag{3.16}$$

$$F_\tau = \tau_w \cdot L_x \cdot L_y \tag{3.17}$$

where ∇p is the pressure gradient defined as $\nabla p = (p_{in} - p_{out})$, and τ_w is the shear stress defined by the wall model. By making these two equations equal it is possible to obtain the expression for the gradient of pressure.

$$\nabla p = \frac{u_*^2}{L_z} \tag{3.18}$$

where u_* is the shear velocity and can be obtained from the logarithmic velocity profile defined by the wall model, by using the imposed velocity $U_{H,\infty}$ at $z = 90m$. The obtained pressure gradient for the surface boundary layer case is $\nabla p = 2.724 \cdot 10^{-4}$.

Now, let us define the friction Reynolds number as following

$$Re_\tau = \frac{\rho u_* L_z}{\mu} \tag{3.19}$$

where ρ is the air density which is $\rho = 1.225kg/m^3$ and μ is the dynamic viscosity taking a value of $\mu = 1.81 \cdot 10^{-5}kg/(m \cdot s)$. Following Equation 3.19 the friction Reynolds number for this case is $Re_\tau \approx 3.5 \cdot 10^7$.

It is also possible to calculate the parameter y_+, an adimensional parameter indicating the size of the cells closer to the walls, and calculated as in Equation 3.20

$$y_+ = y \cdot \frac{\rho u_*}{\mu} \tag{3.20}$$

where y is the absolute distance from the wall. The value obtained for this parameter is $y_+ \approx 10^5$. Both values, usually defined for a channel flow, indicate that the present case is highly turbulent. However, these two parameters are not usually used for wind applications due to its high values, so they will not be taken into account.

In order to gather the important input parameters of the surface boundary layer, they are summed in Table 3.1.

Table 3.1: Setting parameters for surface boundary layer case.

Case	TI	z_0	u_*	∇p
Surface boundary layer	12.8%	0.168 m	0.522	$2.724 \cdot 10^{-4}$

The objective of simulating the surface boundary layer case is to validate the velocity profile imposed by the wall model.

3.3.2 Single wind turbine

This case of study consists on introducing a wind turbine, modelled with an actuator disc, into the surface boundary layer.

In this case, the domain of the flow is $\Omega = [-0.4L_x, 0.6L_x] \times [-0.5L_y, 0.5L_y] \times [0, L_z]$, where $L_x = 16000m$, $L_y = 12000m$ and $L_z = 1500m$. The axis are defined to be x in the streamline direction, y in the streamwise direction and z in the vertical direction. This domain must be larger than the previous case in order to avoid the wake re-entering into the domain due to the periodic boundary conditions. The actuator disc is located at the point $(0, 0, 90)m$, perpendicular to the x axis and a diameter D.

Boundary conditions

The boundary conditions applied to the domain of a single wind turbine are the same as the ones defined for the surface boundary layer case. Even though in this case a disc is placed inside, the domain is large enough so that it does not have any effect in any boundary.

Initial conditions

The initial conditions of the single wind turbine case are exactly the same as the ones in the surface boundary layer case. At the initial time, a logarithmic velocity profile is imposed with a randomly fluctuating component.

Setting the case

In this case of study, the parameters for the numerical simulation can be divided in two different cases. On one hand, a first case of high TI with $TI = 12.8\%$, and a second case of low TI with $TI = 4\%$. In both of the cases the imposed velocity is at hub height, that is $Z = 90m$, and takes a value of $U_{H,\infty} = 8m/s$.

Following Equation 3.15 it is possible to obtain the roughness of the surface for each of these cases, that will change due to its dependence on TI. In the case of high TI case, the

roughness obtained is $z_0 = 0.16822m$, and in the case of low TI the roughness obtained is $z_0 = 1.6629 \cdot 10^{-7}m$.

Regarding the pressure gradient, it is true that an extra force is acting on the domain, which is the actuator disc force. However, it only acts on a control volume inside the domain that does not affect the inflow and outflow boundaries. The driven pressure force and the shear force do act on the totality of the domain and are not affected by the actuator disc force. Therefore, in this case the pressure gradient is calculated following Equation 3.18. For the case of high TI, the pressure gradient is $\nabla p = 1.812 \cdot 10^{-4}$, and for the case of low TI case the pressure gradient is $\nabla p = 1.773 \cdot 10^{-5}$.

The input parameters for both single turbine cases are gathered in Table 3.2.

Table 3.2: Setting parameters for single wind turbine cases.

Case	TI	z_0	u_*	∇p
High TI	12.8%	0.1682 m	0.522	$1.812 \cdot 10^{-4}$
Low TI	4%	$1.663 \cdot 10^{-7}m$	0.163	$1.773 \cdot 10^{-5}$

Wind turbine model

Even though the wind rotor is modelled as an actuator disc, some parameters are needed in order to define its performance. The parameters taken for this actuator disc are the ones corresponding to the National Renewable Energy Laboratories (NREL) 5MW turbine. The main parameters of this wind turbine are gathered in table 3.3.

Table 3.3: NREL 5MW general properties [8].

Power	**Hub height**	**Diameter (D)**	C_t **at 8 m/s**
5 MW	90 m	126 m	0.78

The diameter D will be used from now on as a unit measure for distances inside the domain.

3.4 Meshing

3.4.1 Introduction

The mesh procedure is one of the most important parts of the setup of a problem. In this case, the mesh generation is carried out by means of the in-house meshing code developed in BSC, divided in two parts.

The first part is WindMesh, which generates an structured mesh of the Atmospheric Boundary Layer (ABL) divided in three different zones, from inner to outer: farm, transition and buffer. In this first part, the parameters of the different zones can be defined, as well as the properties for the vertical meshing.

The second part of the meshing procedure is DiscMesh, which generates an structured mesh of the actuator disc and its wake inside the ABL, previously meshed. In it, the parameters like the element size of the wake or the number of elements in the disc can be defined.

3.4.2 Surface boundary layer

The first case to mesh is the surface boundary layer. In this case, only WindMesh is used since there is no actuator disc in the domain. The smaller element size is 25 meters and increases up to 35 meters, being the maximum element length. The mesh is uniform horizontally, meaning that the size of the element does not change at same heights. However, it does change progressively in the vertical direction with a factor of 1.1. In total, this mesh counts with approximately $3 \cdot 10^6$ elements.

3.4.3 Single wind turbine

In the case of placing an actuator disc in the domain the meshing procedure is more complicated. In this case, both WindMesh and DiscMesh are run, introducing a wake mesh with finer elements in order to capture the turbulence happening in the surrounding of the disc. In particular for this case, two meshes have been done, but the size of each zone has been maintained. The dimensions of the farm, transition and buffer are shown in Figure 3.2. The wake region mentioned in the figure is introduced inside the farm zone by DiscMesh, and counts with the smaller elements of the entire domain since it is the region under study.

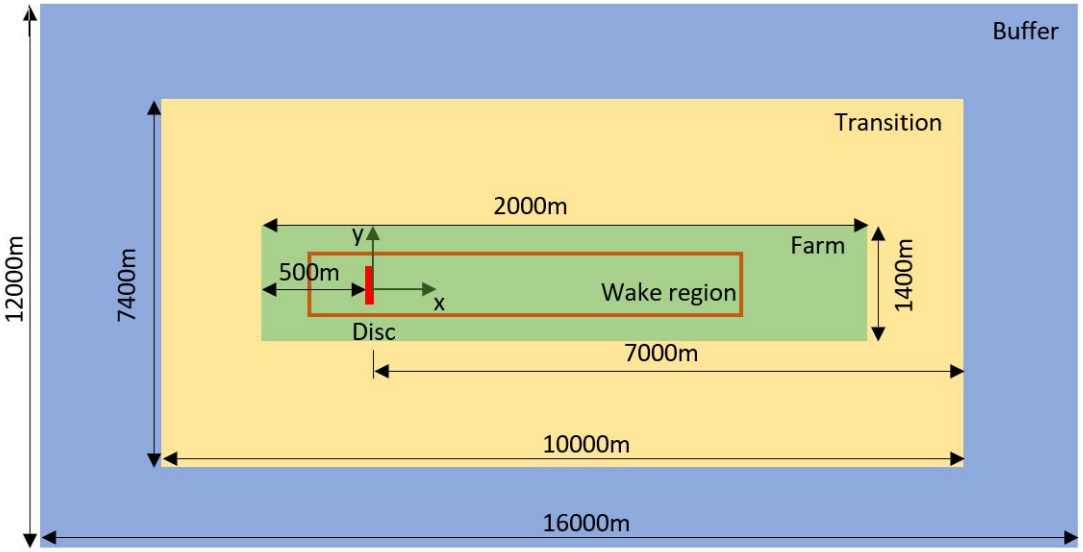

Figure 3.2: Domain structure in WindMesh of the parts and dimensions.

The mesh in the farm and the wake regions are where the smaller elements are found. The size of these elements is a very important parameter since it will define the size of the eddies that form the turbulence. Therefore, with the objective of studying the effect of the element size in the wake and farm regions, two meshes are simulated.

In the first mesh, the buffer has an element size of 40 meters and the element size of the farm

is 30 meters both in x and y direction. In the wake, the minimum element size is $0.06D$, and it increases with a ratio of 1.1 until reaching the background element size. Then, a layer of tetrahedral elements is introduced in order to adapt the wake to the domain mesh. A conic angle of 2^{o} has been implemented in order to avoid interference with the bottom wall and meshing problems. Regarding the disc, it has been discretised with one layer of elements with $0.16D$ width. In total, this mesh counts with $7.2 \cdot 10^6$ elements, and the wake mesh can be seen in Figure 3.3.

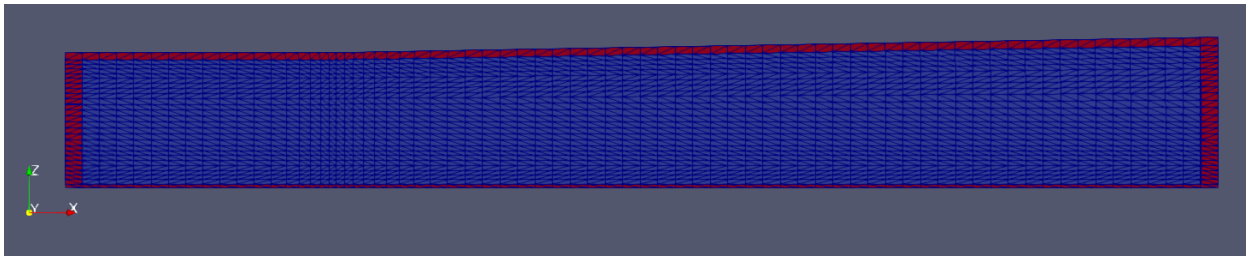

Figure 3.3: Detail of the coarse wake mesh.

A second mesh has been created in order to refine the domain when simulating the case with high TI. In this case, the element size of the farm is 20 meters in x and y direction. In the wake, the minimum element size is $0.04D$, with an increasing ratio in the wake of 1.05 in order to get a smoother transition towards the background. The conic angle has been maintained, and the layers forming the disc have been increased to two, having each one the half of the width with respect to the previous one. In total, this second mesh counts with $10.2 \cdot 10^6$ elements, and the wake region of the mesh can be seen in Figure 3.4.

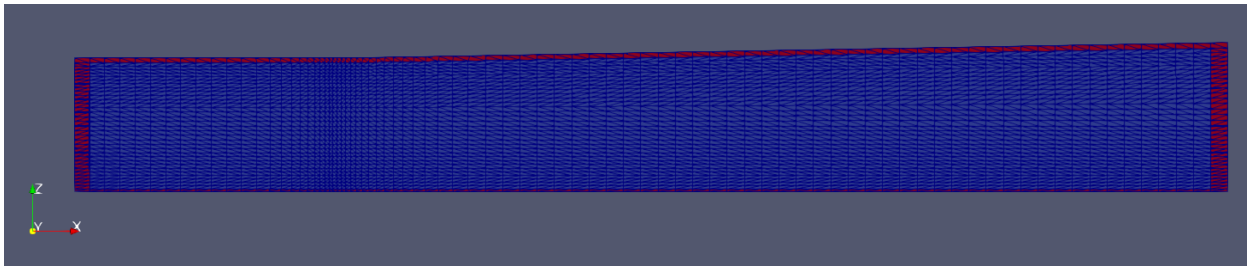

Figure 3.4: Detail of the fine wake mesh.

3.4.4 Mesh summary

In order to have a clearer view of al the meshes created, Table 3.4 gathers the three meshes, with a brief description of the case in which it is applied, number of elements and the size of the smaller element.

Table 3.4: Summary of characteristics of each mesh.

Mesh	**Description**	**Nº of elements**	**Smaller element**
1	Surface boundary layer	$3 \cdot 10^6$	25 m
2	Single wind turbine	$7.2 \cdot 10^6$	$0.06D$
3	Single wind turbine	$10.2 \cdot 10^6$	$0.04D$

3.5 Numerical method

LES equations, using Vreman model, are implemented in Alya and are solved using a Galerkin discretization and a fractional step. The use of a Laplacian operator for the pressure satisfies the inferior-superior condition, and equal interpolation can be used for velocity and pressure. The code is implemented to run in parallel CPUs, capable of running large-scale simulations. An explicit time step is used for LES, using the Runge Kutta method of order 4 [2].

3.6 Computational characteristics

The number of CPUs, Control Processing Units, assigned for a case is a key parameter in terms of computational efficiency. This number depends directly on the number of elements of the case mesh, and since there are different meshes for each case, Table 3.5 gathers the number of CPUs assigned to each case, and the ratio between the number of elements and the number of CPUs.

Table 3.5: Summary of computational characteristics of each mesh.

Mesh	**Nº of elements**	**Nº CPUs**	**Nº elements/Nº CPUs**
1	$3 \cdot 10^6$	768	$4 \cdot 10^3$
2	$7.2 \cdot 10^6$	1536	$4.7 \cdot 10^3$
3	$10.2 \cdot 10^6$	1536	$6.5 \cdot 10^3$

The optimal ratio between number of elements and the number of CPUs should be around $\approx 10^4$, or at least meet the same order of magnitude, in order to optimise the computational capacity. However, in the three meshes under study, this relation is below the optimal ratio, meaning that perhaps the number of CPUs could have been reduced.

An other important parameter in terms of computational characteristics is the time step used for each simulation. This time step Δt is set to meet the Courant-Friedrichs–Lewy condition such as

$$CFL = u\frac{\Delta t}{\Delta x} \approx 2.5 \tag{3.21}$$

where Δx is the length between mesh elements. The time step for the mesh 1

3.6.1 Summary of cases

With the objective of letting more clear the cases and simulations that are going to be run, the following table has been created to gather all the different performed simulations and from which the results in the next section have been taken from.

Table 3.6: Summary of all the cases simulated with important characteristics.

# Case	Description	AD Force	Mesh
1	Surface Boundary Layer	-	1
2	Single turbine, high TI	Constant	2
3	Single turbine, high TI	Constant	3
4	Single turbine, high TI	Calculated with $U_{H,\infty}$ at 3D	2
5	Single turbine, high TI	Calculated with $U_{H,\infty}$ at 3D	3
6	Single turbine, high TI	Calculated with U integrated at the disc	2
7	Single turbine, low TI	Constant	2
8	Single turbine, low TI	Constant	3
9	Single turbine, low TI	Calculated with $U_{H,\infty}$ at 3D	2

3.7 Post-processing

Post-processing the results of the simulations in a correct manner is important in order to minimise the errors. Some aspects to take into account are where the data is being stored or what integration time provides the most reliable results.

The software used Alya is capable of storing certain points, defined by the user, in which the data is stored. These points are called witness points, and they usually are in zones of interest, meaning the parts of the domain in which phenomena under study takes place. The witness points defined in this work contain several lines located at:

- Vertical line at the inlet of the domain.
- Three horizontal lines, crossing the actuator disc at the top height of the disc, at hub height and at the lower height of the disc.
- Three arcs with centre in the hub at distances: 2.5D, 5D and 7.5D.

The method followed to obtain the average values of the variables in the different cases is continuous averaging. Once the solution is believed to have achieved the statistical steady state, that is, the behaviour of the system does not change in time, the results are obtained through three different methods.

The first one consists on having an integration time of 1 hour (physical time) and making directly the average of these values. In this case, larger frequencies are captured due to the wide time integration.

The second one consists on having an integration time of 10 minutes (physical time). This integration time is called bin, and 6 of them are taken in order to compute the average of each of them. Then the total average is done, having the average values of 1 hour. In this case, shorter frequencies can be captured due to the lower integration time.

Finally, the third integrating method is having the same integration time of 10 minutes, but in this case 12 bins are measured. The main objective of having three different ways to integrate in time the solution is to study which method gives the more real and stable results.

In order to evaluate the results obtained with each integration time, it is useful to compare the different shapes obtained for the turbulent kinetic energy (TKE). The TKE is defined as the root-mean-square variation of the velocity, so it is a good indicator of which frequencies are being captures and which are not. Figure 3.5 shows the TKE obtained at hub height when applying a constant force, and compares the three different methods. The case of 1 bin of 1 hour shows higher values of TKE because it captures larger frequency modes of the instantaneous velocity at distances near the disc, between -1D and 2D. Then, the case of 12 bins of 10 minutes shows the lowest values, capturing lower frequencies. The case of 6 bins of 10 minutes shows an intermediate value between the last two.

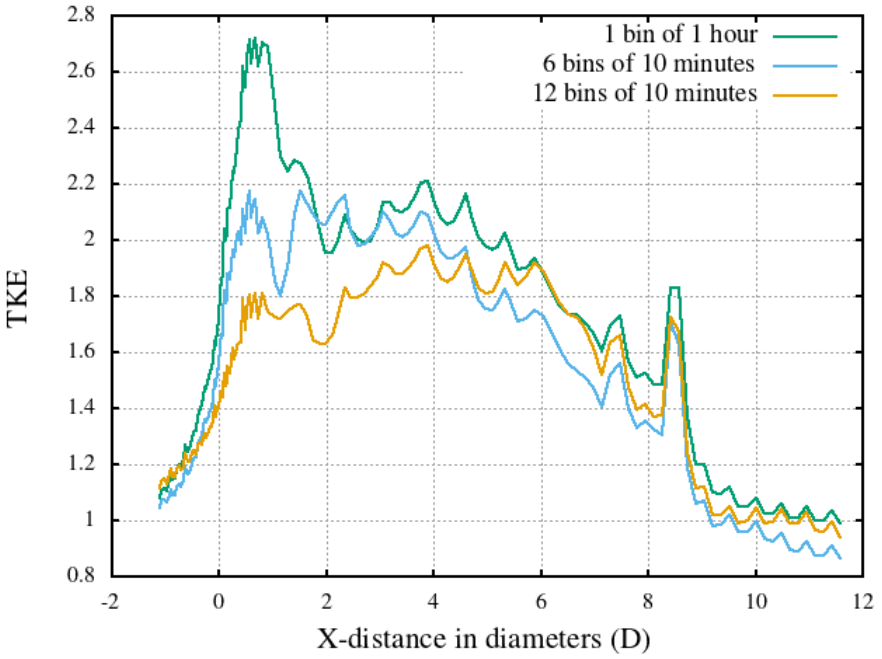

Figure 3.5: TKE at hub height for three different integration times.

Therefore, the post-processing of the results will be done with 6 bins of 10 minutes each because it takes into account the largest frequencies corresponding to shorter times than 10 minutes, and these are the frequencies under interest. The consequence of choosing this method will be the reduction of the standard deviation, due to the shorter averaging time of each bin.

All the simulations have been run for a period of 14 hours, physical time, and the flow statistics were calculated during the last 3 hours of simulation. These amount of run time can also be expressed in flowthroughs, which is the time that the air takes to travel from the beginning to the end of the domain.

In the case of the surface boundary layer, the flowthrough is $t_{FT} = \frac{10000m}{8m/s} = 1250s$. Then, the simulation time is equivalent to 40 t_{FT}, which should be enough to achieve statistical steady state.

In the cases with a single wind turbine, the flowthrough time is $t_{FT} = \frac{16000m}{8m/s} = 2000s$. The simulation time is equivalent to 25 t_{FT}, which should also be enough to achieve the statistical steady state.

3.8 Validation

The results validation of the surface boundary layer is done by observing if the obtained velocity profile is equal to the analytical one, and that the given velocity and turbulence intensity are obtained for a certain height.

The results validation of the single wind turbine is done through comparison with the data provided by Paul Van der Laan, and exposed in [4]. The data provided include the velocity and turbulence intensity of the two single wind turbine cases, and have been of great help when discussing the obtained results.

Chapter 4

Results

In this Chapter 4 the results of the test cases are going to be presented. In first place, the solution of the surface boundary will be explained and commented, followed by the results obtained on the cases of a single wind turbine, with high and low TI. All the results are going to be studied and compared to the reference when possible, in order to validate them.

4.1 Surface boundary layer

In this first case the flow going through the surface boundary layer is resolved. The objective of this first case is to validate the solution given by Alya using Vreman LES model and ensure that the logarithmic profile of the velocity and the expected turbulent intensity values are being achieved. The results shown have been calculated by making the average of planes at constant height, that is horizontal and time averaging.

When simulating the flow inside the surface boundary layer, a logarithmic velocity profile should be obtained in the whole domain. This logarithmic profile is defined by the roughness indicated in Table 3.1 for the case of high TI, achieving a velocity of 8 m/s and an initial estimated turbulence intensity of 12.8% at hub height, which is 90 meters. In the results provided in this section are showing the results obtained for the velocity and turbulence intensity.

The bottom boundary condition is a wall-modelled no-slip boundary, meaning that the height of the element in which the velocity is imposed must be defined. In this case, the first element of the mesh has a height of 3 meters, and the wall distance, where wind speed is measured to obtain the shear stress, is 15 meters. The simulation results below this height are not valid, but above 15 meters the velocity is adapted satisfactorily. Since the hub height is 90 meters, it can be considered that the section of the profile in which does not match the logarithmic shape will not have a significant effect on the results. Figure 4.1 shows the comparison between these two velocities, and it can be observed how the obtained profile is adapted to the logarithmic one, considering it as correct for the surface boundary layer flow simulation.

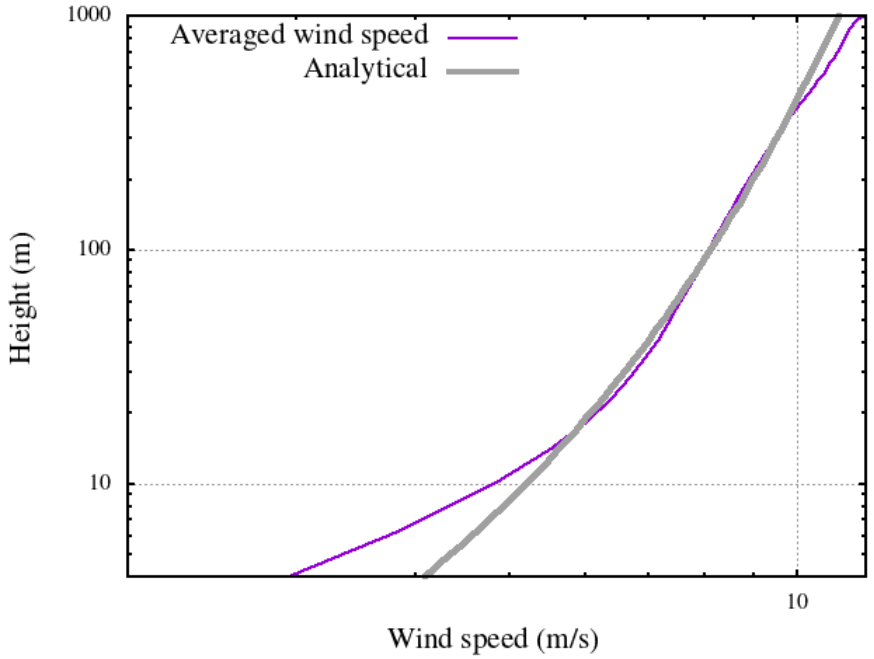

Figure 4.1: Average velocity profile comparison between analytical and obtained in surface boundary layer case.

Another aspect to validate is the turbulence intensity obtained at hub height. Figure 4.2 shows the turbulent intensity profile. In it, the turbulence intensity obtained at hub height is of $TI \approx 10.5\%$. This TI differs from the estimated one a 25% (estimated one is $TI = 12.8\%$) , which is normal since the estimated one was calculated using $k - \varepsilon$ RANS equations, and the present simulation is a LES. It is important to note that the imposed TI is lower than the one expected, so it could lead to some difference in the results validation.

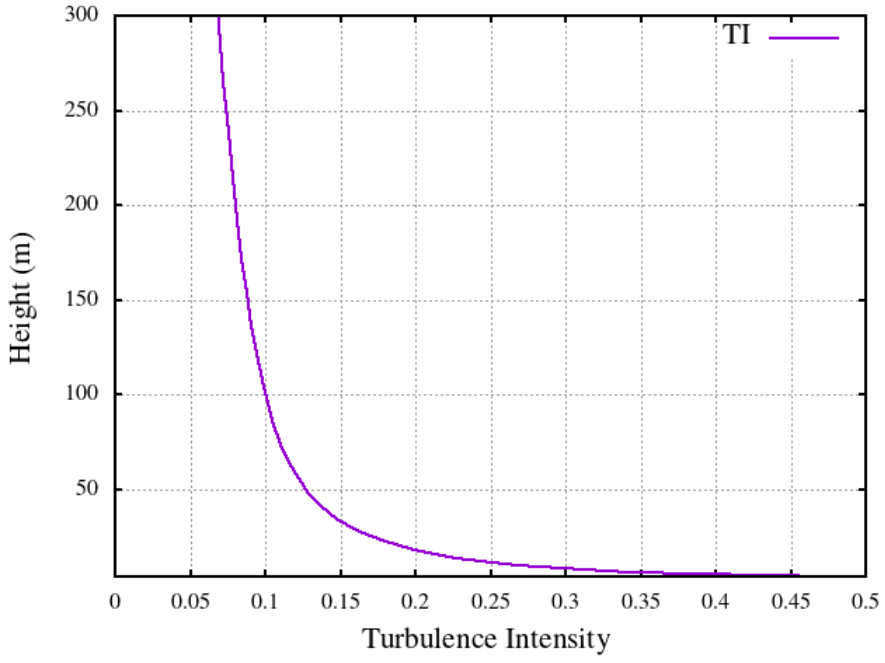

Figure 4.2: Turbulence intensity vs. height for surface boundary layer case.

The complete domain with the average velocity of the flow is represented in Figure 4.3, where the lowest values take place in the bottom wall of the domain, while the highest ones the place in the top wall, as expected. Looking at the inlet boundary, it can be observed that the flow in the streamwise direction is not uniform, and some structures parallel to the streamline direction are formed., which are called streaks.

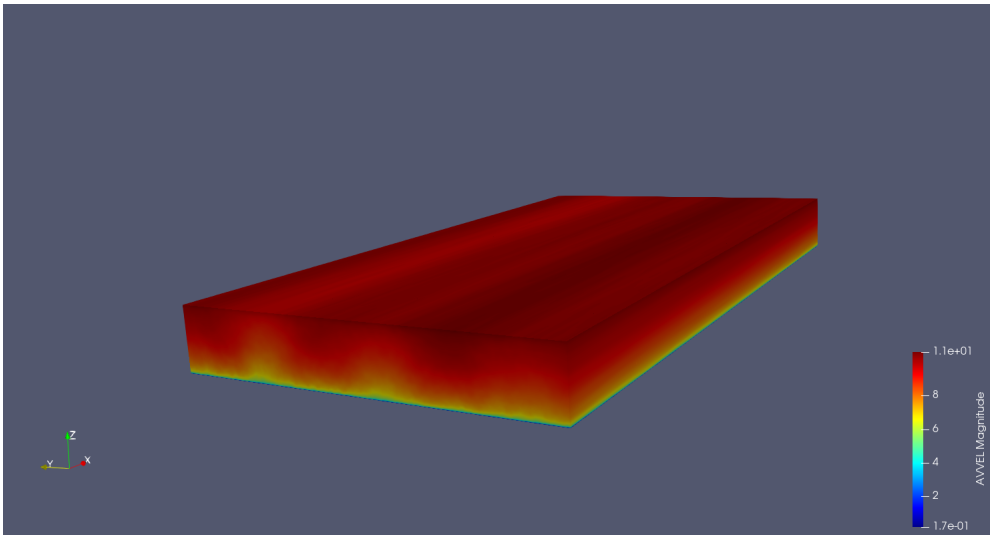

Figure 4.3: Average velocity in surface boundary layer domain.

The objective of this case was the setup of the velocity profile and the turbulence intensity in order to obtain their values when having undisturbed flow. In the next section, a wind turbine is placed inside the surface boundary layer, so the obtained values in this case can be taken as reference.

4.2 Single wind turbine

The results of the single wind turbine cases are going to be presented in this section. The velocity wake deficits and the turbulence intensity results are plotted at hub height with respect to the relative wind direction and matching the downstream locations measured by Van der Laan et al [4], which are 2.5D, 5D and 7.5D. Before showing the results of each case, some discussion about the average time of the results and the type of force applied is done in order to decide what are the most suitable

4.2.1 Actuator disc force comparison

As explained in Section 3.2, the actuator disc force can be modelled in several ways. In the present work, three different forces have been simulated and studied. In order to compare them, the period between 8 and 10 hours of physical time is chosen.

For the high TI case, the three different methodologies to calculate the force are compared: constant force related to a constant inflow wind speed of 8m/s, force calculated considering the undisturbed wind speed as the upstream velocity at 3D, and finally the force calculated with the Glauert theoretical relation by measuring the mean volumetric wind speed in the rotor

disc. From these three, the last methodology is the only one which is suitable over complex terrain. Figure 4.4 shows the evolution in time of each of the undisturbed wind velocities between 8 and 10 hours of simulation. The constant force is represented with a straight velocity line because it does not change with time, but the other two velocities fluctuate with similar amplitudes, and therefore it is inferred that the force should fluctuate also with similar amplitude. The three velocities are oscillating around the same value, which is 8 m/s.

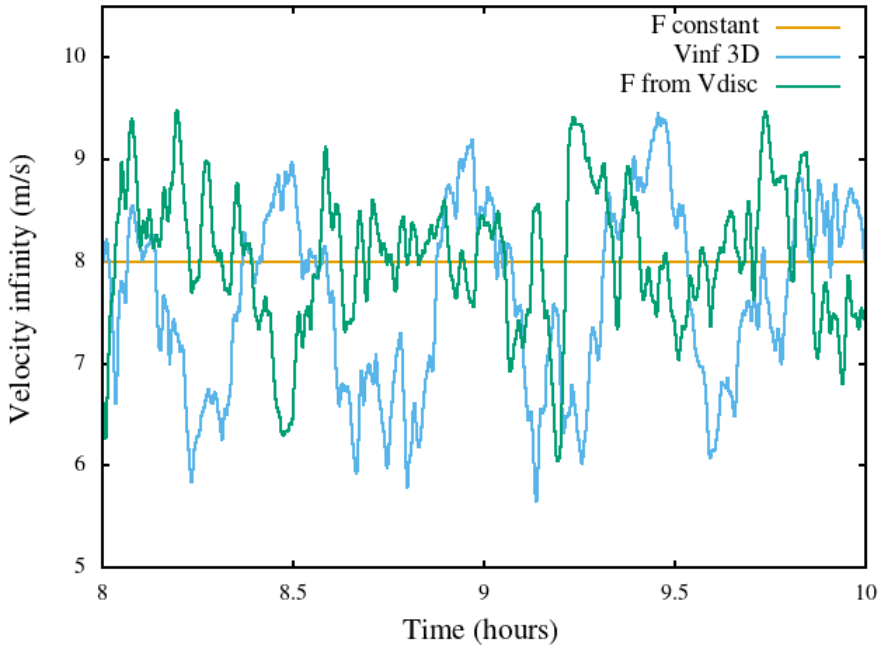

Figure 4.4: Time evolution in high TI case of undisturbed wind velocity for three different forces: constant, calculated with velocity at 3D and calculated with integrated velocity at the disc.

In the low TI case only two forces are compared: constant force and force calculated with upstream velocity at 3D. Figure 4.5 shows the evolution of these two undisturbed velocities, in which the constant velocity is represented as a straight line, but the force calculated with upstream velocity at 3D shows fluctuations.

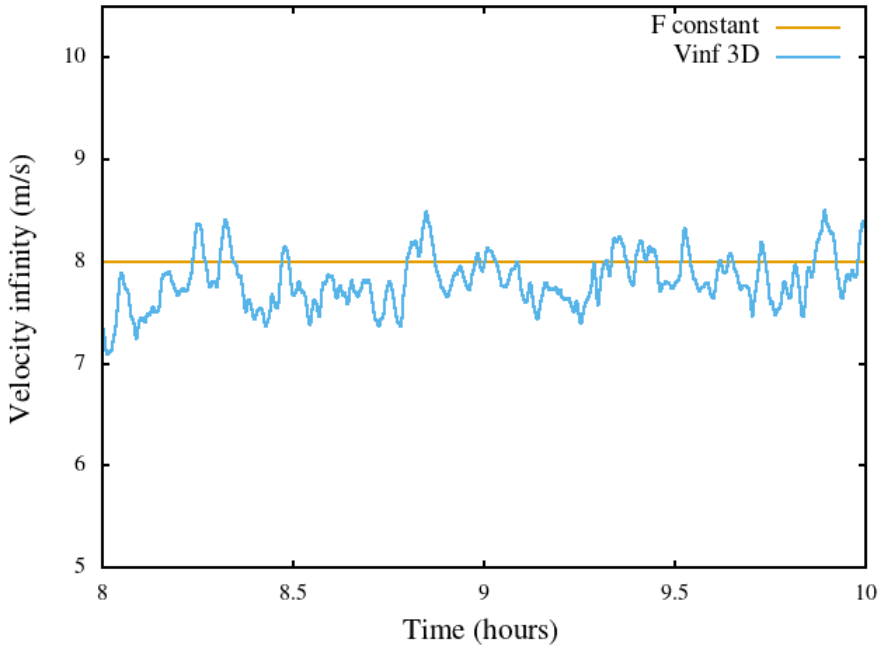

Figure 4.5: Time evolution in low TI case of undisturbed wind velocity for two different forces: constant and calculated with velocity at 3D.

Although the force depending on the undisturbed velocity taken at 3D fluctuates, the amplitude of the undisturbed velocities for the low TI case is much lower than the obtained one for the high TI case. Figure 4.6 shows both undisturbed velocities for low and high TI cases, and the difference in amplitude can be clearly seen.

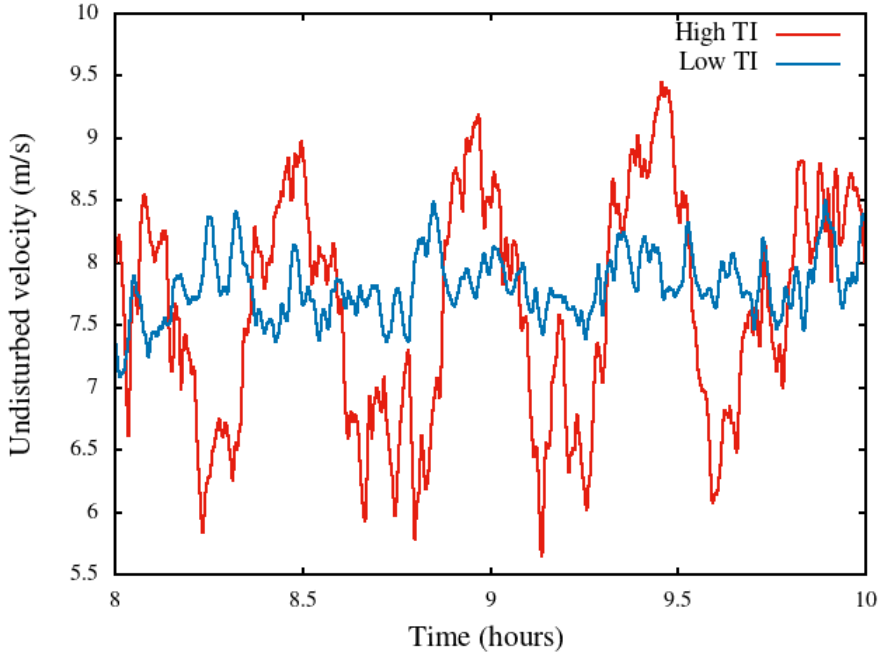

Figure 4.6: Comparison of time evolution of undisturbed wind velocity between high and low TI cases.

The high TI case is characterised by its high turbulence, which makes very difficult to get converged results and the values will fluctuate more than in the low TI case. The high TI case is driven by a larger pressure gradient than the low TI case, which is proportional to the introduction of turbulent kinetic energy to the domain. Making an equilibrium hypothesis, the averaged TKE dissipation of the high TI case is higher than in the low TI case. This larger TKE dissipation means a smaller Kolmogorov length, and then the high TI problem will need a finer mesh than the low TI problem.

When comparing the velocity obtained at the disc with each method, Figure 4.7 shows its time evolution for a time period of 2 hours. The velocity obtained with the constant force shows higher amplitudes and more fluctuations in comparison with the other two, which have similar amplitudes. This larger amplitudes introduced by this force are going to introduce a higher turbulence intensity than a normal wind turbine. Part of the reason of this phenomena is that there is not a prescribed inflow and that the boundary conditions are periodic. There is no low stability, so the results may differ from the validation results. Even though the results from the reference are obtained with a constant force, an inlet velocity is imposed with a constant mean horizontal velocity, without streaks, that evolves with very low frequencies.

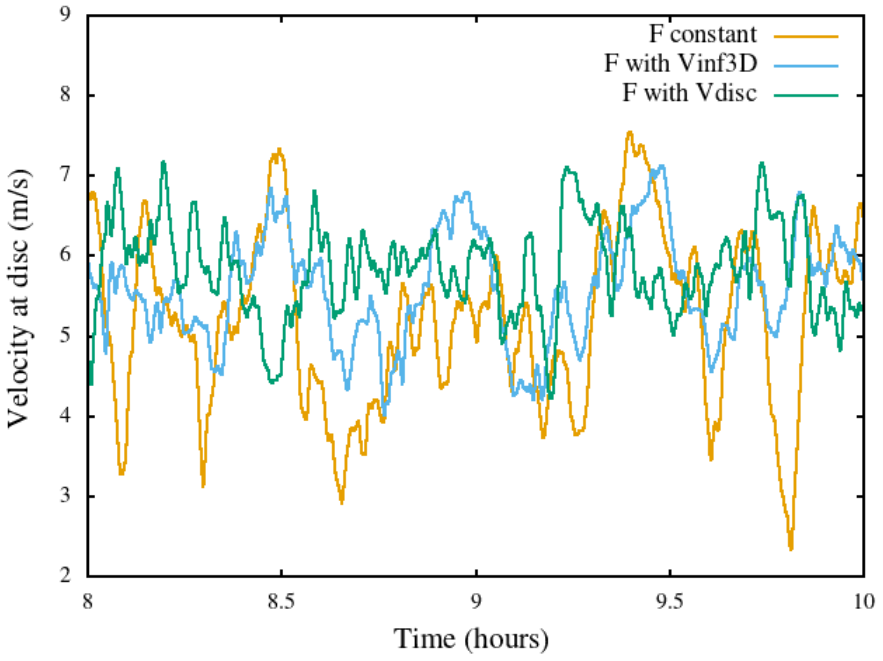

Figure 4.7: Time evolution of the velocity at the disc for the three methods to obtain the force: constant, calculated with velocity at 3D and calculated with integrated velocity at the disc.

It is also interesting to observe how each force behaves in terms of obtaining the undisturbed velocity and relating it to the velocity at the disc. Figure 4.8 shows the case in which the velocity is taken at a distance of 3D from the disc. In this case, there is a clear relation between the free stream velocity and the velocity at the hub: they are related through a coefficient which is almost constant, making them very similar in terms of shape.

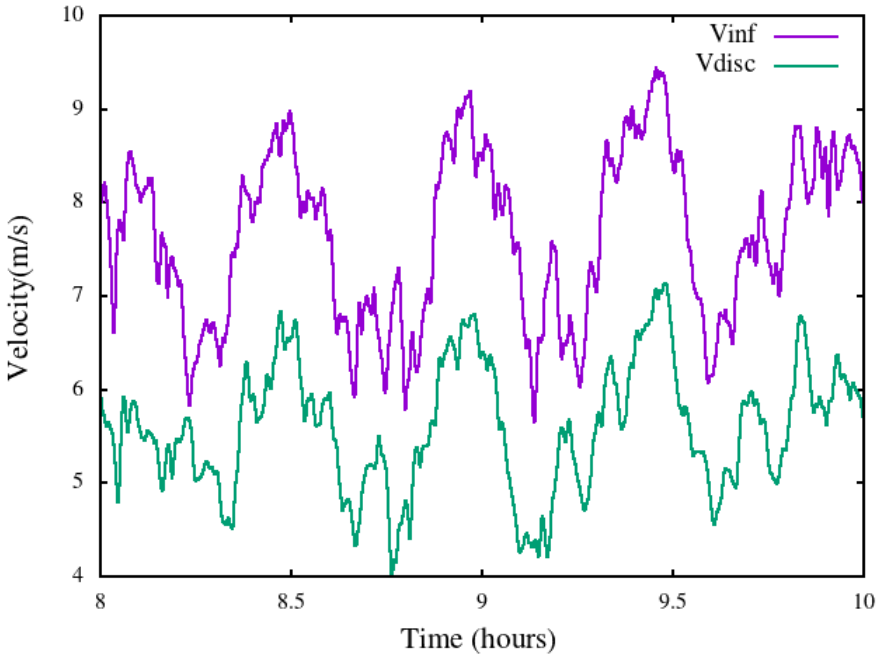

Figure 4.8: Time evolution of unperturbed velocity and velocity at the disc when $U_{H,\infty}$ taken at 3D upwind of the rotor.

Figure 4.9 shows the relation between the free stream velocity and the velocity at the disc when it is integrated in the disc and averaged in 1 minute. In this case, both velocities fluctuate with the same pattern as the previous case, but now the frequencies are higher. Again, the relation between the undisturbed wind velocity and the velocity at the disc is practically constant.

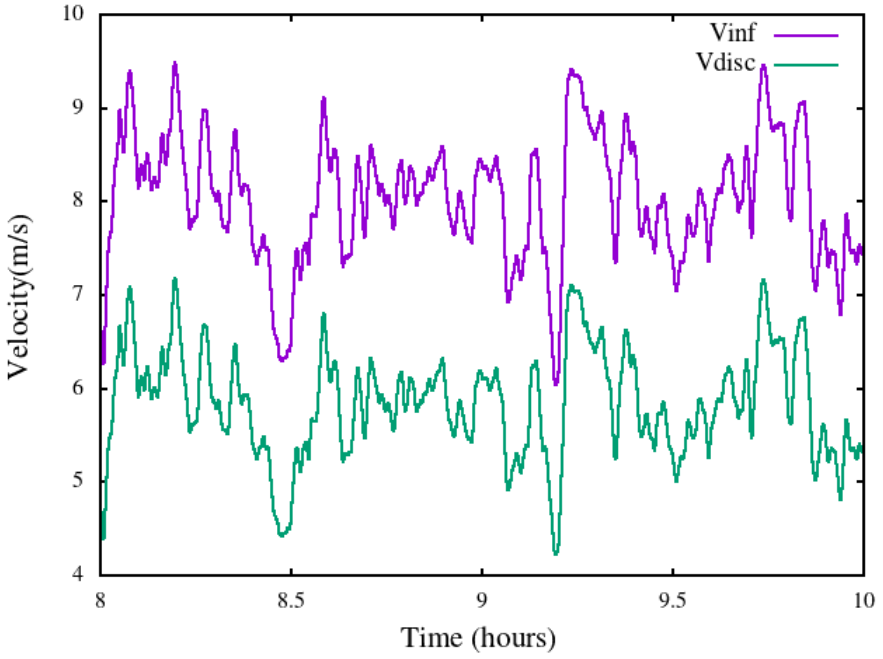

Figure 4.9: Time evolution of unperturbed velocity and velocity at the disc when $U_{H,\infty}$ taken integrating the velocity at the disc.

In both cases, the one with the velocity measured at 3D from the disc and the one with the velocity integrated at the disc, the mean velocity is the same. Figure 4.10 shows the evolution in time of the ratio between the unperturbed velocity and the velocity at the disc. It can be observed that both ratios oscillate around the same mean value. However, the ratio from the force calculated with the Glauert relation varies less than the ratio from the velocity taken at 3D from the disc.

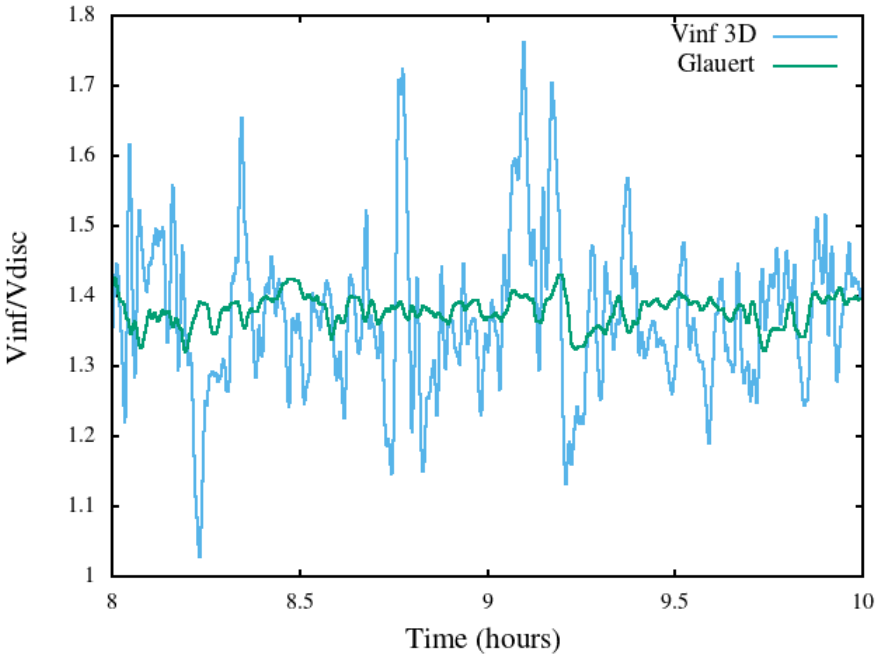

Figure 4.10: Comparison of time evolution of the ratio between the unperturbed velocity and velocity at the disc for the two forces: calculated with unperturbed velocity at 3D and velocity integrated at the disc.

Observing the three ways of obtaining the actuator disc force, it has been shown that the most suitable and realistic is the one which is calculated with the free stream velocity at 3D from the disc. This velocity is taken from a distance in which the velocity is not perturbed and therefore, is the most realistic way to calculate the force, since it will detect all the real fluctuations happening in the flow. The constant force could not be considered for this work because it is not adapted to the velocity and causes big fluctuations, giving inaccurate results and being difficult to converge, and the force calculated following Glauert theoretical relation could be a good approximation, but due to its theoretical nature it is more suitable to apply the chosen method, which has a more realistic basis.

4.2.2 Convergence study

In order to evaluate the performance of each mesh, convergence must be studied. To do so, the evolution of the hub velocity in each case can be compared for different times. If the solution has converged, the results should not change from hour to hour, meaning that they do not depend on time anymore. In all the cases the methodology used to calculate the force has been taking the undisturbed velocity from a distance of 3D from the disc.

The first mesh to be tested is the coarse one, which corresponds to mesh number 2 in Table 3.4. In the case of high TI, the simulation has run for 14 hours, physical time, with this mesh. Figure 4.11 shows the average hub horizontal velocity in each of the three last hours of simulation, where the results, if the statistical convergence has arrived, should not change. However, in the Figure 4.11 it can be seen that before the disc the velocity suffers a slight variation in the last hour with respect to the previous one, meaning that convergence has not been achieved. Therefore, this case should have been run more simulation time, but due to the lack of time it was not possible. Anyway, the results obtained are going to be compared to the ones in reference, assuming that an error can be made because of not having achieved the statistical steady state.

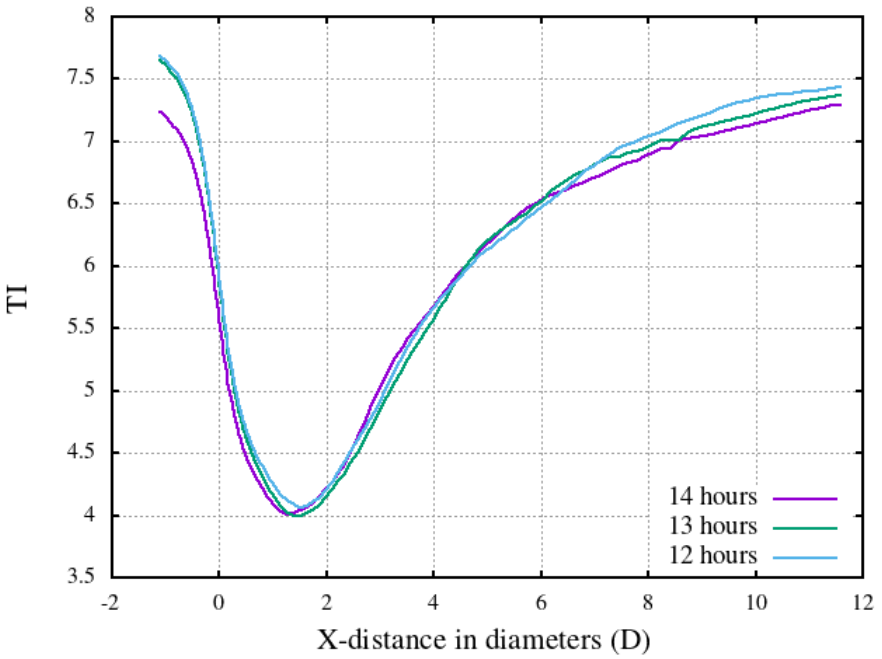

Figure 4.11: Evolution of the average velocity at hub height for high TI case with coarse mesh.

In the case of low TI, Figure 4.12 shows the evolution of the hub velocity for the three last hours of simulation. In this case, the solution practically does not vary, having achieved the statistical state. Therefore, the results from this simulation can be taken as converged.

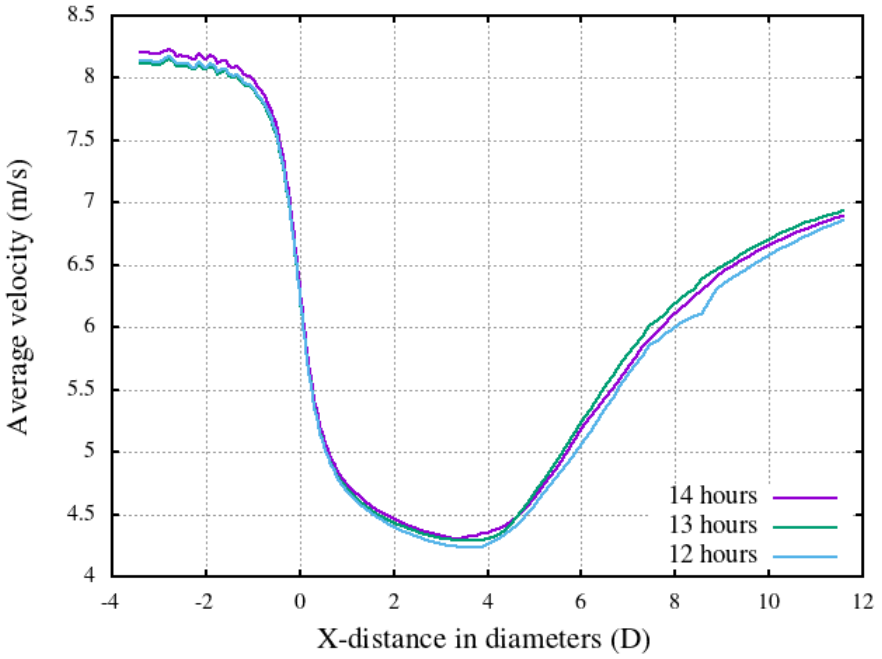

Figure 4.12: Evolution of the average velocity at hub height for low TI.

The high TI case was simulated with the second mesh, which is the finer one, in order to observe if reducing the scale size more accurate resutls are achieved. In this case the simulation has run for 14 hours, and Figure 4.13 shows the evolution of the horizontal velocity at the hub for the three last hours. Clearly, the statistical steady state has not been achieved, and due to the lack of time the simulation could not be run for more hours. This case in particular is going to be treated carefully, since the variation on the average velocities from different hours differ much more than the ones from the high TI case with coarser mesh.

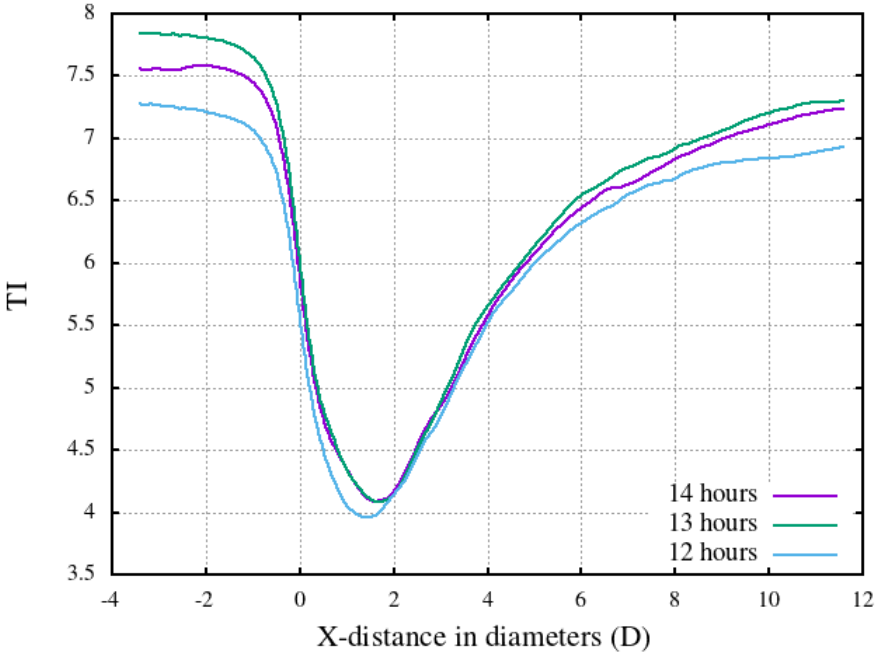

Figure 4.13: Evolution of the velocity at hub height for high TI case with the finer mesh.

4.2.3 Turbulence intensity

The turbulence intensity is an indicator of how much the flow is fluctuating with respect to the mean wind speed. In this section, the TI of each case is under study in order to obtain the real value, and discuss how much it differs from the estimated one.

High TI case

The high TI case is a particular one due to its high amount of turbulence. The TI varies considerably from a certain group of bins to the next one since it does not converge completely. Figure 4.14 shows the turbulent intensity obtained for the three last hours of simulation. As it can be seen, the values differ from one hour to another, meaning that convergence has not been achieved.

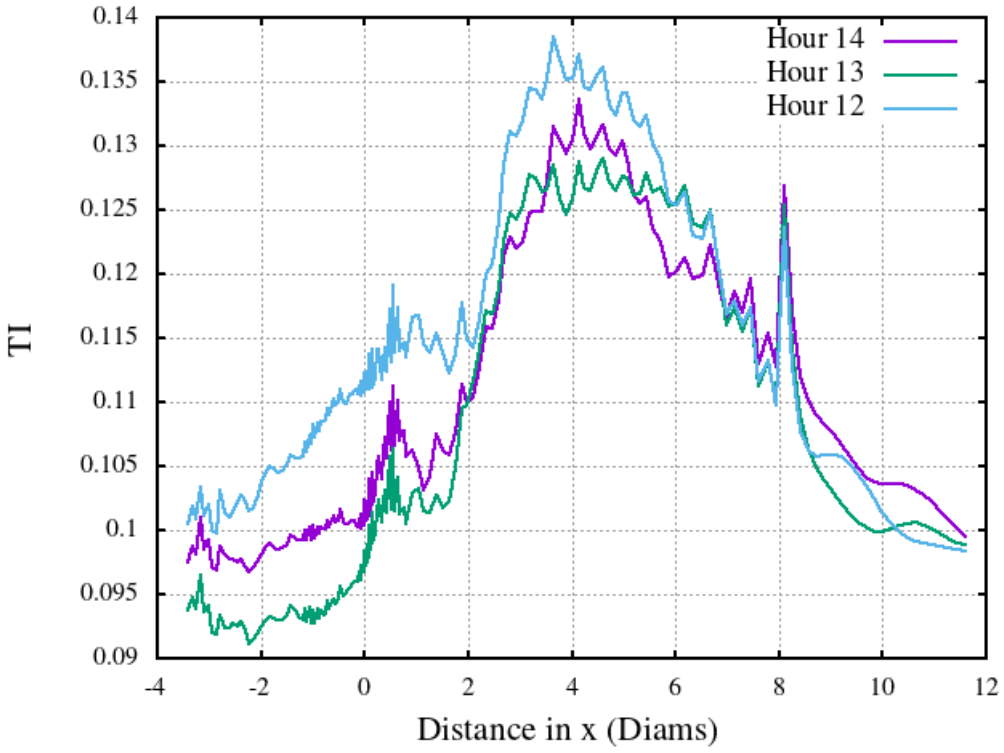

Figure 4.14: Comparison of TI values obtained for the last three hours of simulation time in the high TI case with fine mesh.

However, an estimation can be done by observing the TI values obtained for each of the three averages. At distance around $-3D$ the flow is undisturbed and therefore the value of TI should match with the one obtained in the surface boundary layer case. By taking a mean value of the three average results, turbulence intensity in this case is $TI \approx 9.8\%$. Comparing this value to the one obtained in the surface boundary layer ($TI = 10.5\%$), it only differs a 7% from it, which can be considered as a good approximation taking into account the high oscillations in this case.

When approaching the disc, the turbulence intensity starts suffering higher fluctuations due to the presence of the induction zone. It is in the mid-wake, around 3D, where the TI takes the higher values and reaches the peak. Then, it starts decreasing in the far-wake. An important

feature in this figure is the high peak at 8.3D. This irregularity is due to the abrupt change of mesh size given by WindMesh and DiscMesh. Figure 4.15 shows the end of the wake mesh, that is adapted to the farm through tetrahedral elements. The change of size of these elements takes place at 1050 meters, which coincides with the distance at which the peak happens in Figure 4.14. The increase of TI is explained by the change in size of the scales. When this peak is overcome, the turbulence intensity decreases again since the flow is recovered.

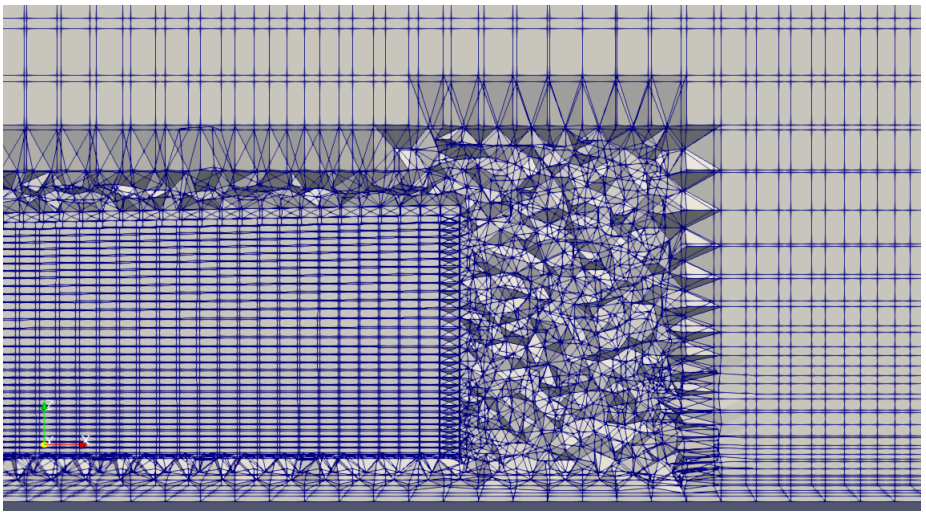

Figure 4.15: Detail of the mesh in the intersection between the wake and the farm mesh.

Low TI

The case of low TI achieves faster the statistical steady state, having results with less fluctuations than those from the previous case. Figure 4.16 shows the evolution of the turbulence intensity for this case, and in which the TI obtained for this case is 3.5% , a 12% than the one estimated that was 4%.

The TI in this case starts from 3.5% and starts to increase when entering in the induction zone of the disc. The peak now is achieved in the mid-far wake, around 6D, corresponding to a longer wake than in the high TI case. Here, it can also be seen the peak at 8.3D from the disc, which again corresponds to the change of element size in the mesh previously shown.

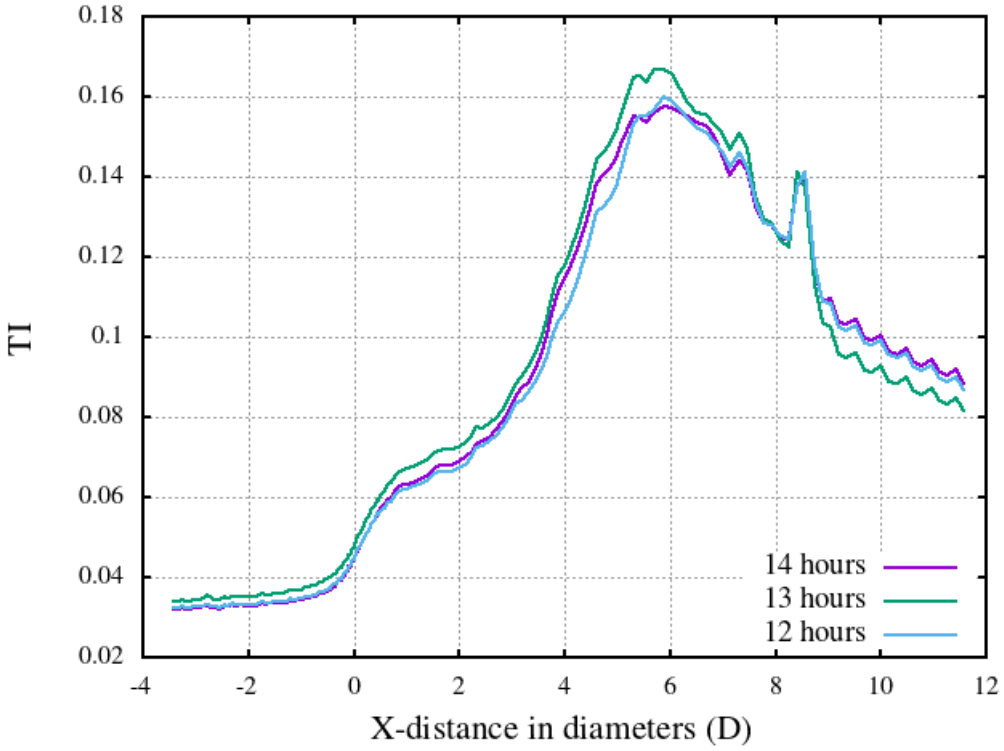

Figure 4.16: Comparison of TI values obtained for the last three hours of simulation time in the low TI case.

4.2.4 Wake validation

This section is focused on validating the main features of the turbulence phenomena when having a wind turbine: turbulence intensity and velocity deficit in the wake. In this case, the results obtained are going to be compared with those from Van der Laan et al [4]. This comparison must be done carefully, since the boundary conditions and the force of each case are different. Van der Laan imposes a mean flow profile at the inlet as a boundary condition and models a constant force with tangential and axial components, simulating the rotational effects of the disc. However, in this work the force has only axial component, periodic boundary conditions are imposed and the inlet mean velocity profile suffers low frequency variations in time and space. Despite this differences, the comparison can be very useful to understand what features differentiate the results.

High TI

The results obtained in the wake have been taken at the arcs located at downstream distances from the disc of 2.5D, 5D and 7.5D.

Regarding the wake deficit, the results show an asymmetry, which is a characteristic feature of non-converged results. In both cases, for coarse and fine mesh, this asymmetry is present, meaning that both cases should have been simulated more time until achieving the statistical steady state. However, in the near wake (2.5D) the results are very close to the reference ones. It is in the mid and far wake where the results start to differ more from the reference. In general terms, the coarse mesh case is closer to the reference results than the fine mesh case.

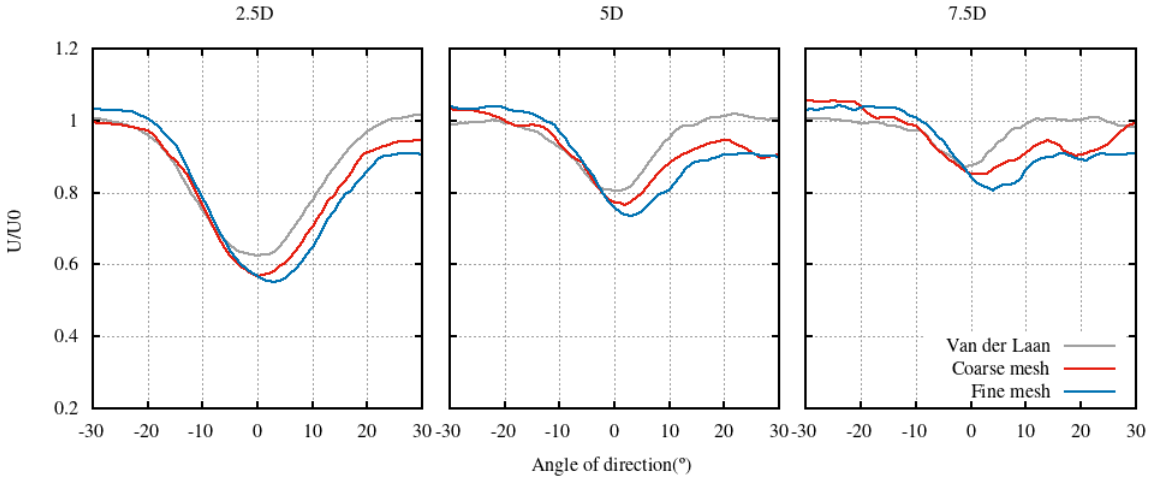

Figure 4.17: Velocity deficit ($U/U_{H,\infty}$) for three distances from the disc in the case of high TI.

In the case of turbulence intensity at the wake, the obtained results underpredict it at all downstream distances. The results from the coarse mesh and the ones form the fine mesh are very similar now, taking very similar values. The only similarity between the reference values and the obtained ones is the shape of the TI, which shows a double peak structure and a slight asymmetry. Nevertheless, the difference in values is evident, so the obtained results cannot be considered as valid in this case.

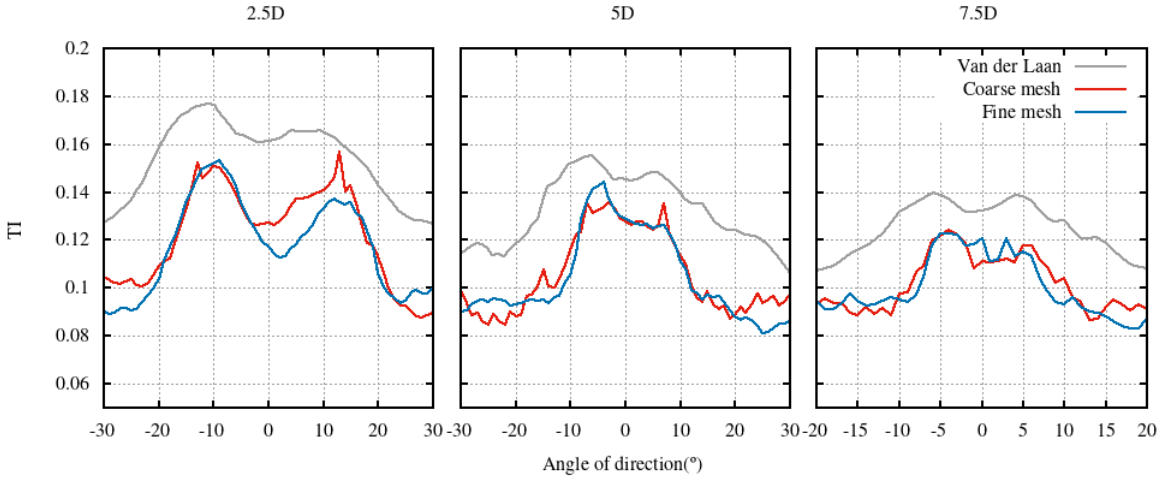

Figure 4.18: Turbulence intensity (TI) for three distances from the disc in the case of high TI.

Low TI

The results obtained in the wake have been taken at downstream distances from the disc of 2.5D, 5D and 7.5D, like the previous case, and they have been compared against the data from Van der Laan [4].

The results obtained for the near wake seem to be predicting the same values of velocity deficit as the Van der Laan results. However, the obtained ones are not able to reproduce the velocity deficit shape in the near wake, which is an effect of the rotational forces. This is

normal, since Van der Laan's force has tangential component and the one in this work only has an axial component.

In the mid wake, at a distance of 5D, the results obtained overpredict the velocity deficit, since it shows a bigger difference of velocity than the results from Van der Laan. This difference could be explained by the difference in turbulence intensity respect to the reference case, that could lead our results to have longer wakes.

In the far wake, at a distance of 7.5D from the disc, the results are very similar to those from the reference, validating these results for the case of low TI.

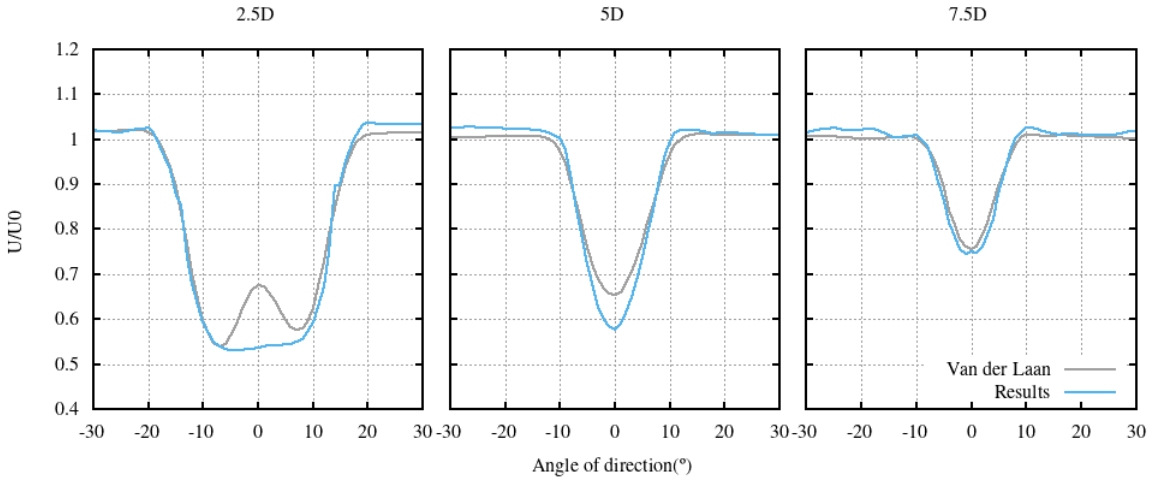

Figure 4.19: Velocity deficit ($U/U_{H,\infty}$) for three distances from the disc in the case of low TI.

Regarding the turbulence intensity, at the near wake (2.5D) it is underpredicted, having higher values for the reference. However, the shape is captured, providing the double peak form. This difference could be explained by the difference on TI values, giving lower turbulence intensity at the near wake.

In the mid wake it seems that the obtained results are approaching the reference ones, but still there is a slight difference where the obtained results are underpredicting the TI.

In the far wake the obtained results slightly overpredict the reference values, by overpassing them. However, the shape and the results can be considered very similar.

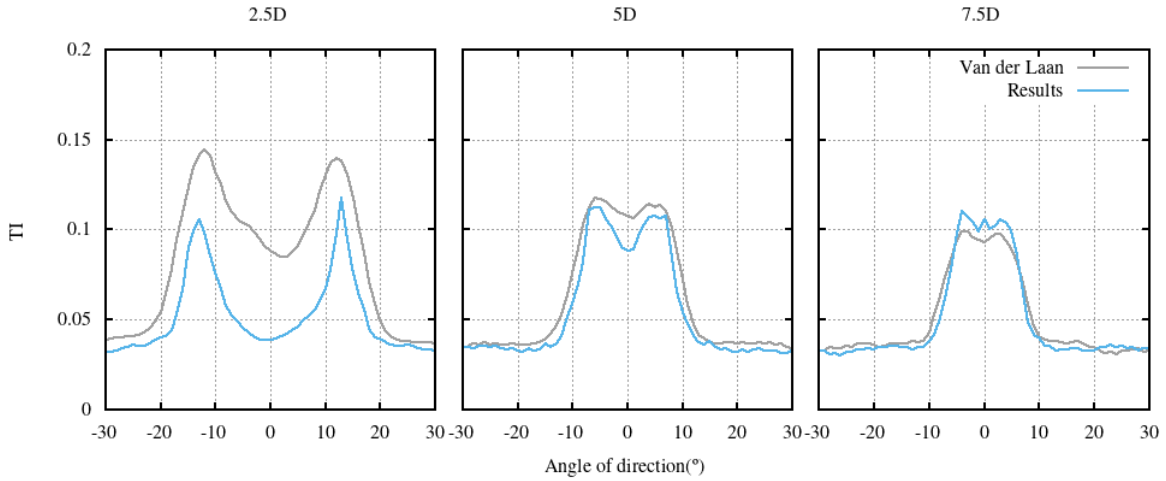

Figure 4.20: Turbulence intensity (TI) for three distances from the disc in the case of low TI.

In general, the results for the low TI case are very similar to the ones from the reference. It is true that some differences are found in terms of shape, like the double peak due to rotational forces, or in terms of values, sometimes differing slightly. However, taking into consideration the difference in TI, which for the reference is $TI = 4\%$ and for the obtained ones is $TI = 3.5\%$, the results can be considered reliable.

4.2.5 Comparison between low and high TI

The high TI and low TI cases differ on the turbulence intensity imposed on the flow, so it is interesting to compare what the effect of this difference is.

In the first case, the average velocity integrated in the last hour of simulation is shown in Figure 4.21 for high TI and in Figure 4.22 for low TI. The figures show an upstream distance of -500 meters (4D) and a downstream distance up to 2000 meters (16D). When comparing both average velocities, a clear difference is seen: the wake for the low TI case has a larger mixing length than the one in the high TI case.

In Figure 4.21 the wake has approximately a distance of 1100 meters (9D), where the velocity recovers and takes the same value as the one before the disc. On the other hand, Figure 4.22 shows a larger wake that even at 2000 meters (16D) still persists, so the flow takes longer to recover. The exact distance at which the wake is dissipated is at The wake for lower turbulence intensity is longer, since the flow takes a longer distance to mix with the surrounding air outside the wake.

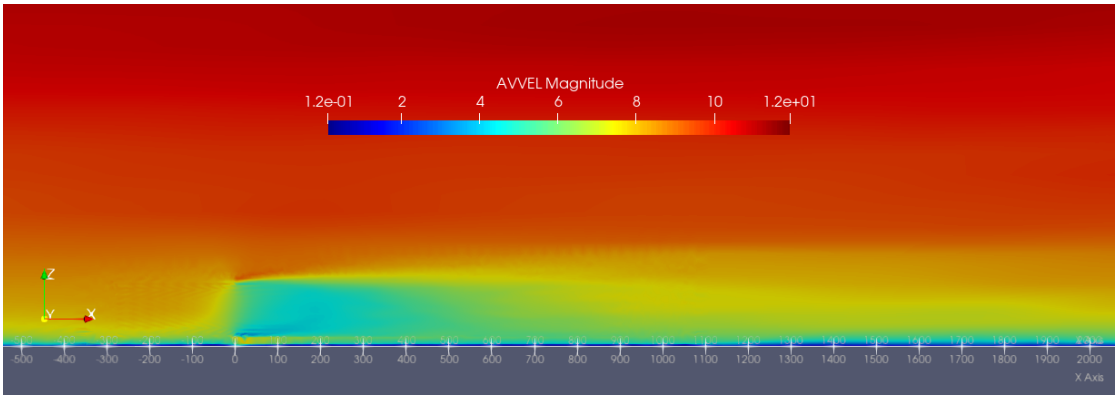

Figure 4.21: Average velocity for high TI case.

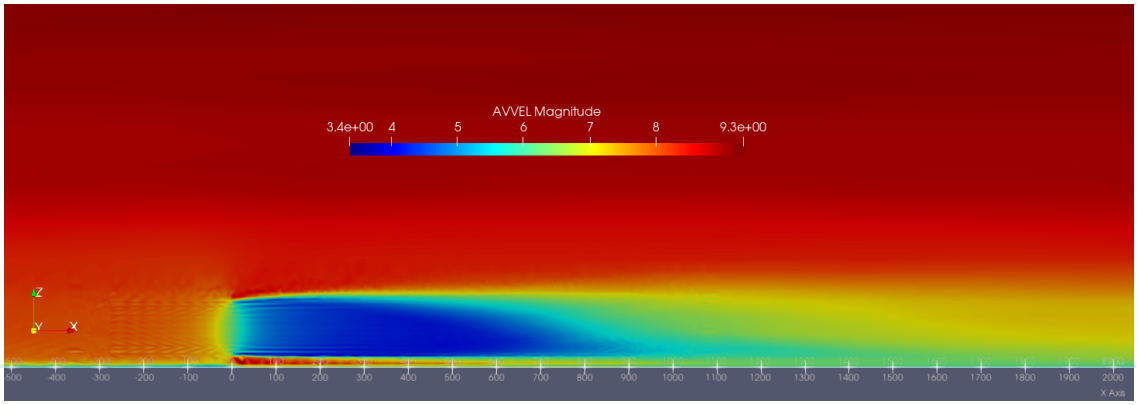

Figure 4.22: Average velocity for low TI case.

The wake deficit in the transversal direction can also be compared by making cuts of the disc at distances 2.5D, 5D and 7.5D. Figures 4.23 and 4.24 show these cuts for high and low TI respectively.

In the case of high TI, at the near wake the velocity takes a value of $5m/s$ approximately, and then in the mid and far wake it progressively dissipates. Specifically, at the far wake it is almost completely dissipated.

However, in the case of low TI, at the near wake a lower velocity can be observed in the whole disc diameter, being around $4m/s$, and showing that the velocity deficit is higher for the low TI case. Furthermore, the circular shape of the disc is maintained until the far wake, meaning that it takes longer to dissipate than 7.5D.

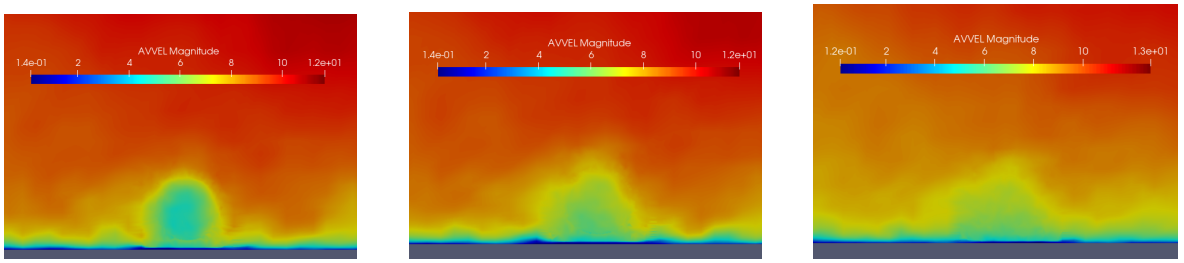

(a) 2.5D (b) 5D (c) 7.5D

Figure 4.23: Average velocity at distances 2.5D (a), 5D (b) and 7.5D (c) from the disc for high TI case.

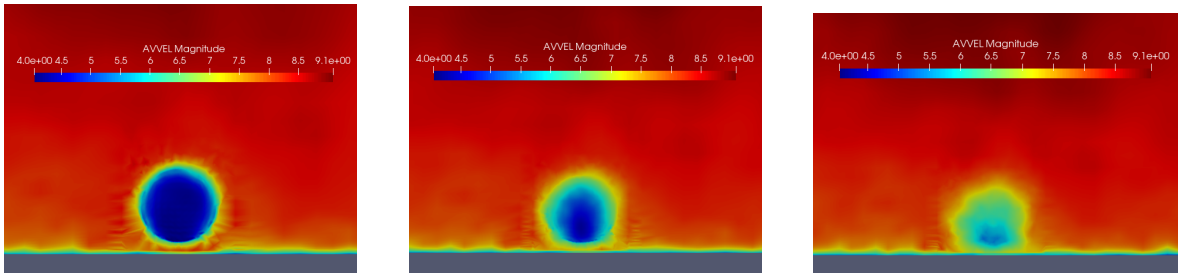

(a) 2.5D (b) 5D (c) 7.5D

Figure 4.24: Average velocity at distances 2.5D (a), 5D (b) and 7.5D (c) from the disc for low TI case.

Chapter 5

Budget

5.1 Costs summary

In this section, the total budget of making the project is presented. Table 5.1 shows the different packages that carry an economic charge and have been performed in this work.

Table 5.1: Partial cost of each task and total cost of the project.

Task	**Price per unit**	**Units**	**Total**
CFD MESH	0,05 €/h·cpu	144	7€
MN4 SIMULATIONS	0,05 €/h·cpu	182784	9140€
POSTPROCESS	0,05 €/h·cpu	432	32 €
REPORT	0.3€/kWh	90 kWh	27 €
COMPUTER	1400 €	1	1400 €
STUDENT WORK HOURS	15€/h	410	6150 €
TUTOR WORK HOURS	30€/h	150	4500 €
		TOTAL	**21256 €**

Chapter 6

Conclusions

6.1 Results

The results obtained can be analysed by dividing them in the three main test cases.

In the case of the surface boundary layer, the objective is achieved by obtaining a velocity profile adapted to the analytical one, and meeting approximately the turbulence intensity imposed. This test case is useful in order to ensure that the logarithmic profile, later applied on single wind turbine case, suits the imposed boundary conditions.

In the case of high TI the results are very complicated to analyse. The high amount of turbulence makes it very difficult to achieve the statistical steady state, so the results cannot be considered valid. However, they give an estimation of what values they will take. Definitely, more simulation time is needed in order to have reliable results in this case.

The case of low TI is more stable in terms of turbulence, so the statistical steady state is achieved. The statistical results show that convergence is obtained by not varying in the last hours of simulation. The wake validation results show similarity to the ones from the reference in [4], taking almost the same values. The main difference between them can be found in the near wake, where the velocity deficit has a different shape due to the lack of rotation of the disc, and the turbulence intensity TI is underpredicted due to the lower value obtained. In general, it can be said that the implemented model has been validated for this case.

The forces comparison was also an important part of the present work, where different methods for representing the actuator disc force were studied. The results obtained match with theoretical background explained in Section 3.2. The force calculated with constant velocity shows a constant force, and the velocity at the disc suffers more fluctuations. Then, between the other two forces, the one calculated with the undisturbed velocity at a distance of 3D upstream the disc shows the more real behaviour, taking into account the real perturbations of the flow. Because of this reason, it was the force chosen to compare with the reference results.

In general, the results obtained are in agreement with what was expected, so they can be considered as satisfactory.

6.2 Future work

The work done is limited by the available time, which is four months. From the end of the project, several possibilities were proposed in order to continue with it.

The most clear future work is to restart the simulations of high TI cases in order to study if statistical steady state is achieved. This could be very useful in order to obtain valid results for this case, and therefore being able to compare them with the reference in a proper way.

One of the improvements of the work that could be done is to introduce a pressure controller. What this makes is to detect the fluctuations and vary the pressure gradient in order to adjust the flow and reduce the oscillations. This would have been very useful in terms of having a more stabilised undisturbed velocity, and therefore having more stable actuator disc forces.

Another possible future work would be the adjustment of the TI. As previously said in the report, it is possible to start an iterative process, starting from the estimated roughness, in order to achieve the same turbulence intensity as the results from the reference. This would have eliminated the possible error from having different TI and the results could have been better compared.

In terms of expanding the study present in this project, a line to continue would have been the addition of one or more turbines. It would be very interesting to study how the wake behaves when encountering a second disc, or even to study how the air behaves in a wind farm, where several wind turbines are interacting with each other.

Bibliography

1. KOMUSANAC, Ivan; BRINDLEY, Guy; FRAILE, Daniel; RAMIREZ, Lizet. *Wind energy in Europe: 2021 Statistics and the outlook for 2022-2026*. 2022. Tech. rep. Wind Europe.
2. ÁVILA, Matías; GARGALLO-PEIRÓ, Abel; FOLCH, Arnau. A CFD framework for offshore and onshore wind farm simulation. *Journal of Physics: Conference series*. 2017, p. 854.
3. SANDERSE, B.; PIJL, S.P.van der; KOREN, B. Review of computational fluid dynamics for wind turbine wake aerodynamics. *Wind Energy*. 2011, vol. 14, pp. 799–819.
4. LAAN, M. Paul van der; SORENSEN, Niels N.; RETHORÉ, Pierre-Elouan; MANN, Jahob; KELLY, Mark C.; TROLDBORG, Niels; SCHEPERS, J. Gerard; MACHEFAUX, Ewan. An improved k-ϵ model applied to a wind turbine wake in atmospheric turbulence. *Wind Energy*. 2015, vol. 18, pp. 889–907.
5. WISE, Adam S.; NEHER, James M. T.; ARTHUR, Robert S.; MIROCHA, Jeffrey D.; LUNDQUIST, Julie K.; CHOW, Fotini K. Meso- to microscale modeling of atmospheric stability effects on wind turbine wake behavior in complex terrain. *Wind Energy Science*. 2022, vol. 7, pp. 367–386.
6. VREMAN, A. W. An eddy-viscosity subgrid-scale model for turbulent shear flow: Algebraic theory and applications. *Physics of Fluids*. 2004, vol. 16, pp. 3670–3681.
7. SØRENSEN, J. N. *General momentum theory for horizontal axis wind turbines*. Springer, 2016.
8. JONKMAN, Jason; BUTTERFIELD, S.; MUSIAL, W.; SCOTT, G. *Definition of a 5-mw reference wind turbine for offshore system development*. 2009. Tech. rep. National Renewable Energy Laboratory.